

Discotic Receptors: Ion Sensing and Switching

Discotic molecules are of great interest, because of their potential to form fascinating supramolecular architectures. Their strong π - π interactions lead to the high electron mobilities which are essential for the eco-friendly organic photovoltaic cells or transistors. Other potential applications of discotic materials include the fabrication of organic electronic devices such as organic light emitting diodes (OLEDs), field effect transistors (FETs), photovoltaic solar cells, one dimensional conductors, gas sensors and molecular receptors. However, numerous possibilities exist for the use of novel self-assembled architectures based on discotic molecules in the host-guest chemistry such as for metal recognition¹, ion induced self-assembly and sensing of electron deficient nitroaromatic explosives. Keeping in view the importance of discotic molecules in material and supramolecular chemistry, synthesis of discotic molecules is very important. Thus, in the present investigation we have design and synthesize various discotic molecules based on terphenyl and triphenylene core and evaluate their photophysical properties and binding behaviour towards different analytes.

Objectives of the proposal

- 1 Design and synthesis of polyaromatic derivatives
- 2 Evaluation of behaviour of these derivatives as receptors for cations and anions and their use as molecular switches

Work Done

On the basis of research work, we have divided the following sections:

- 1. Terphenyl-phenanthroline conjugate as a Zn^{2+} sensor: $H_2PO_4^-$ induced tuning of emission wavelength**
- 2. Triphenylene based receptors for the recognition of metal ions, anions and nitroaromatic explosives**
 - (i) Triphenylene to supertriphenylene: New chemodosimeter for fluoride ions**
 - (ii) Aggregates of Triphenylene Based Chemosensing Ensemble for Sensitive Detection of Cyanide Ions in Aqueous Medium**
 - (iii) Carbazole Substituted Triphenylene Derivative for the Sensitive Detection of Nitroaromatic Explosives**
 - (iv) Fluorescent Aggregates of AIEE active Triphenylene Derivatives for the Sensitive Detection of Picric Acid**
 - (v) Aggregates of triphenylene derivative as reactor for the preparation of gold nanoparticles**

(vi) Aggregates of Gallic Acid Substituted Triphenylene Derivative for the Sensitive Detection of Trinitrotoluene in Aqueous Medium and in Vapour Phase

3. Thiacalix[4]arene-fluorescein based receptor for detecting CN^- and Cu^{2+} ions and construction of a sequential logic circuit

1. Terphenyl-phenanthroline conjugate as a Zn^{2+} sensor: H_2PO_4^- induced tuning of emission wavelength

Recently, there is an active effort to develop supramolecular systems that simultaneously bind both the cation and the anion. In order to accomplish the above goal, we envisaged that derivatizing the terphenyl framework with imine and phenanthroline moiety should give a host capable of interacting with both cations and anions. We were interested to incorporate phenanthroline moiety in our ligand design as phenanthroline is also an ideal candidate for applications in complexation studies with cations owing to its structural features such as planarity, rigidity as well as intense fluorescence and applications in the synthesis of herbicides, pharmaceuticals, and analytical probes. Thus, we designed and synthesized a macrocyclic Schiff base **5** based on terphenyl incorporating phenanthroline moieties which shows selective binding behavior for Zn^{2+} ions.

Suzuki Miyaura cross coupling of compound **1** with compound **2** catalyzed by Pd (II) furnished diamine **3** in 55% yield. Condensation of diamine **3** with 1.0 mol equiv. of phenanthroline dialdehyde **4** in ethanol (100 ml) gave compound **5** in 77% yields (**Scheme 1**).

Scheme 1

The structure of compound **5** was confirmed from its spectroscopic and analytical data. The ^1H NMR spectrum of compound **5** showed one singlet (12H) for methoxy protons, one singlet (4H) and two doublets (4H, 4H) for phenanthroline protons, one singlet (4H) and two doublets (8H, 8H) for terphenyl protons and one singlet (4H) for imino ($\text{N}=\text{CH}$) protons. In the FAB mass spectrum, parent ion peak was observed at 1041 (M^+) corresponding to the condensation product **5**.

The binding behavior of compound **5** toward different cations (Pb^{2+} , Hg^{2+} , Ba^{2+} , Cd^{2+} , Ag^+ , Zn^{2+} , Cu^{2+} , Ni^{2+} , Co^{2+} , K^+ , Mg^{2+} , Na^+ and Li^+) was investigated by UV-Vis and fluorescence spectroscopy. The UV-Vis spectrum of compound **5** exhibited absorption bands at 217, 284 and 374 nm in THF. Among the various metal ions tested, the addition of Zn^{2+} ($30\ \mu\text{M}$) ions, resulted in the formation of a red-shifted ($\Delta\lambda = 56\ \text{nm}$) weak band at 430 nm with a clear isosbestic point at 398 nm (**figure 1**). This is attributed to the interactions of Zn^{2+} ions with nitrogen atoms of imino and phenanthroline moieties leading to the intramolecular charge transfer (ICT) from the phenanthroline moiety to imino units.

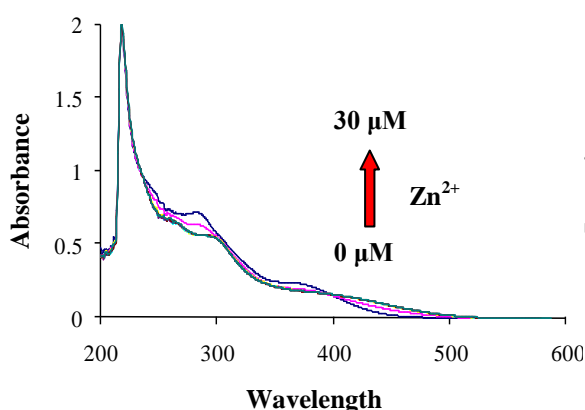


Figure 1: UV-Vis spectra of receptor **5** ($10.0\ \mu\text{M}$) on addition of Zn^{2+} ions ($30.0\ \mu\text{M}$) in THF.

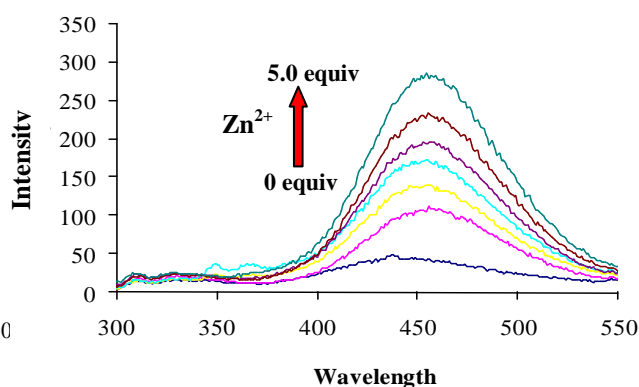


Figure 2: Fluorescence spectra of receptor **5** ($2.0\ \mu\text{M}$) on addition of Zn^{2+} ions ($5.0\ \text{equiv}$) in THF as solvent; $\lambda_{\text{ex}} = 300\ \text{nm}$.

In the fluorescence spectrum, the compound **5** ($2.0\ \mu\text{M}$) exhibited a weak emission band centered at 438 nm when excited at $\lambda_{\text{ex}} = 300\ \text{nm}$ (**figure 2**). This weak emission from compound **5** is due to photo-induced electron transfer (PET) from the imino nitrogens to the photo excited phenanthroline units which leads to poor emission. On addition of zinc ions ($5\ \text{equiv.}$), a significant fluorescence enhancement (10 folds) along with red shift of 19nm occurred leading to the formation of an emission band at 457 nm. The fluorescence quantum yield (Φ_{F}) of compound **5** in the free and Zn^{2+} -bound state was found to be 0.01 and 0.25 respectively.² This is attributed to the modulation of the photo-induced charge transfer (PCT) process induced by binding of Zn^{2+} ions with nitrogen atoms of imino and phenanthroline moieties. Under the same conditions as used for Zn^{2+} ions, we also tested the fluorescence response of compound **5** to other metal ions (Pb^{2+} , Hg^{2+} , Ba^{2+} , Cd^{2+} , Ag^+ , Cu^{2+} , Ni^{2+} , Co^{2+} , K^+ , Mg^{2+} , Na^+ and Li^+) and as shown in **figure 3 (series 1)**, no significant change in fluorescence occurred in the presence of these metal ions. To test

the practical applicability of compound **5** as a Zn^{2+} selective sensor, competitive experiments were carried out in the presence of Zn^{2+} ions at 25 μM mixed with the other metal ions at 100 μM and as shown in **figure 3 (series 2)**, no significant variation in the fluorescence intensity was found by comparison with and without other metal ions. The detection limit was found to be 100 nM which is sufficiently low for the detection of submillimolar concentrations of Zn^{2+} ions as found in many chemical systems.

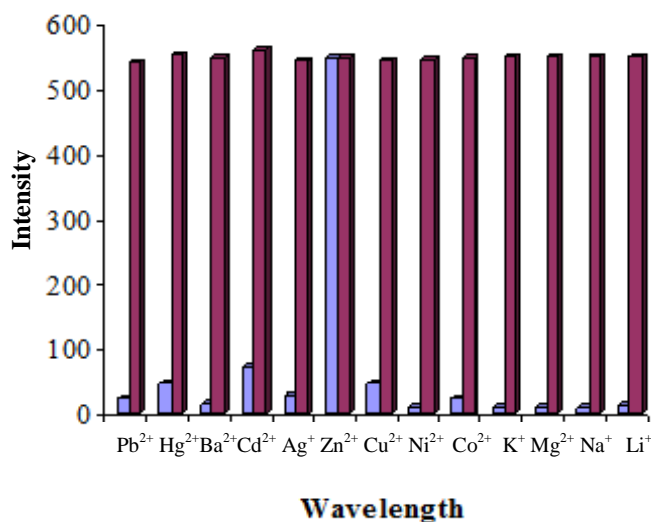


Figure 3: Series 1 showing fluorescence enhancement ratio $(I-I_0/I_0) \times 100$ of receptor **5** (2.0 μM) upon addition of different metal ions (5.0 equiv) and **series 2** showing competitive selectivity of receptor **5** towards Zn^{2+} in the presence of other metal ions (100.0 equiv).

Having done this, we were interested to gain insight into the binding behavior of **[5-Zn]** complex toward various anions (F^- , Cl^- , Br^- , I^- , CH_3COO^- , HSO_4^- , NO_3^- , H_2PO_4^-), as chemosensing ensemble approach is a kind of competitive approach for the design of fluorescent chemosensors for anions. We carried out the fluorescence titration experiments of **[5-Zn]** complex toward different anions with tetrabutylammonium as counter cation. Among all the anions tested, the change in the fluorescence intensity of **[5-Zn]** complex was observed on addition of F^- , CH_3COO^- , and H_2PO_4^- ions. The addition of all three anions F^- (10.0 equiv), CH_3COO^- (10.0 equiv) and H_2PO_4^- (10.0 equiv) to the solution of **[5-Zn]** complex in THF led to fluorescence quenching and finally reaching emission corresponding to that of compound **5** (**figure 4**). Further, to observe, whether the binding of three anions is reversible in nature we again added Zn^{2+} ions (100.0 equiv) to the solution containing **5-Zn.CH₃COO⁻**/**5-Zn.F⁻**/**5-Zn.H₂PO₄⁻** species. The fluorescence emission was enhanced at 438 nm in case of F^- and CH_3COO^- ions while a blue shifted broad band appeared at 418 nm in case of H_2PO_4^- ions (**figure 5**). The above fluorescence

behavior of F^-/CH_3COO^- ions is attributed to the binding of these anions with Zn^{2+} ions of **[5-Zn]** complex resulting in the decomplexation of Zn^{2+} ions, due to which the

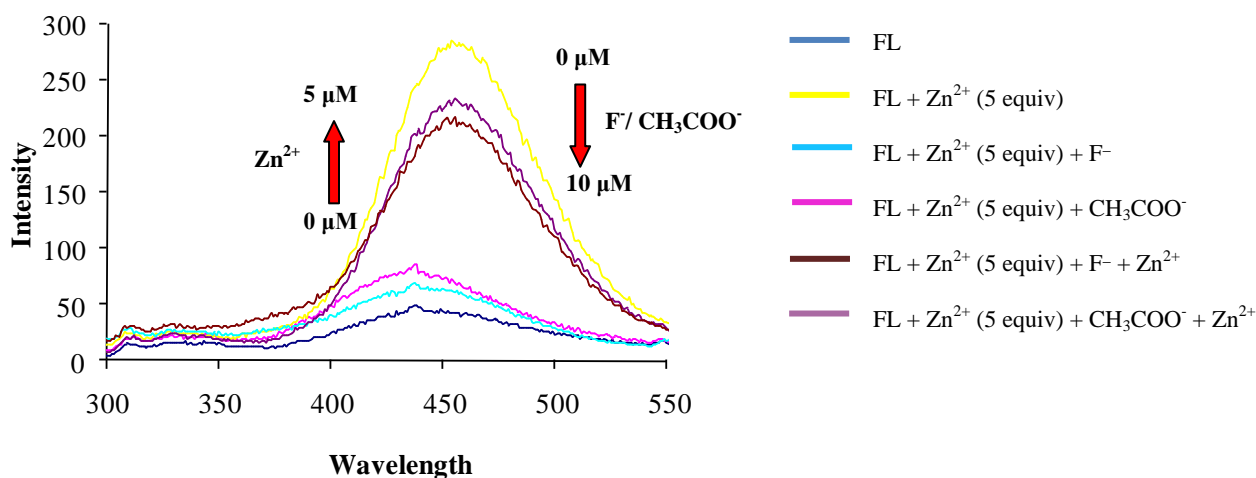


Figure 4: Fluorescence spectra of receptor **5** (2.0 μ M) on addition of F^- and CH_3COO^- ions after Zn^{2+} ions (5.0 equiv) in THF as solvent; $\lambda_{ex} = 300$ nm.

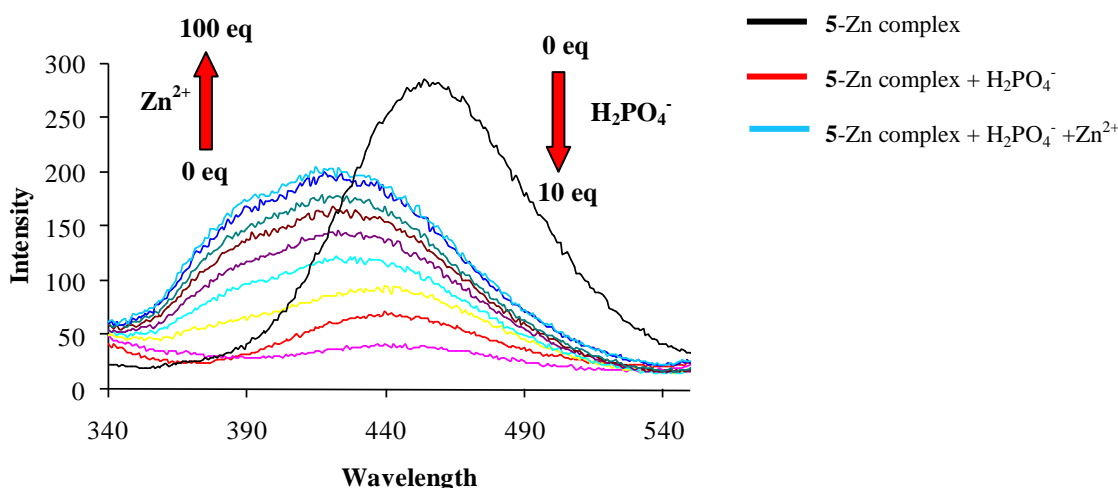


Figure 5: Fluorescence spectra of receptor **5** (2.0 μ M) on addition of Zn^{2+} ions (100.0 equiv) in presence of $H_2PO_4^-$ ions (10.0 equiv) in THF as solvent; $\lambda_{ex} = 300$ nm.

fluorescence emission of the **[5-Zn]** complex gets quenched. The revival of fluorescence intensity on further addition of Zn^{2+} ions in case of F^-/CH_3COO^- is ascribed to the binding of Zn^{2+} ions with nitrogen atoms of imine and phenanthroline moieties. However, in case of $H_2PO_4^-$, we observed contrasting behavior which may arise due to binding of electron rich oxygen atoms of $H_2PO_4^-$ to the complexed form of Zn^{2+} ions. It is expected that $H_2PO_4^-$ binding simply weakens the Zn-N interactions.

The above results can be explained on the basis of hypothesis that in the absence of

H_2PO_4^- , binding of Zn^{2+} ions with imino nitrogens of receptor **5** is strong enough which may affect the electron density on methoxy oxygens. Whereas when we added H_2PO_4^- to the **5**-Zn complex, owing to the hydrogen bonding of H_2PO_4^- with Zn^{2+} ions, binding of Zn^{2+} ions with imino nitrogens get weakened which may not reduce the electron density on oxygens and hence this site can efficiently bind to additional Zn^{2+} ions.

In conclusion, we synthesized a highly selective fluorescent chemosensor for Zn^{2+} ions utilizing terphenyl–phenanthroline based macrocycle as a scaffold.

2. Triphenylene based Receptors

(i) Triphenylene to supertriphenylene: New chemodosimeter for fluoride ions

Among discotics, triphenylenes are the most widely studied for their liquid crystalline behaviour. However, structural features controlling mesophase type and stability are found to be extremely subtle and conjugated substituents that are able to extend triphenylene's π -system supported mesophase formation. Thus, supertriphenylenes are found to have stable columnar mesophase as compared to their respective triphenylene analogues. In this present work, we have developed a simple strategy for synthesis of supertriphenylene derivative from triphenylene derivative using fluoride induced cyclization.

The Suzuki-Miyaura coupling of hexabromotriphenylene **6** with boronic ester **7** furnished the extended triphenylene derivative **8** in 81% yield (**Scheme 2**). The ^1H NMR spectrum of compound **8** in CDCl_3 showed four singlets (36H, 36H, 54H and 54H) corresponding to the protons of the *tert*-butyldimethylsilyl (TBS) group, one singlet, one doublet and one multiplet (6H, 6H, 12H) for aromatic protons. The FAB mass spectrum showed a parent ion peak at m/z 2248 (M^+). These spectroscopic data corroborate the structure **8** for this compound. Further the treatment of triphenylene **8** with tetrabutylammonium fluoride and its subsequent reaction with triflic anhydride furnished supertriphenylene **9** (72%) where three C-C bonds are formed in single step.

Scheme 2

Based on these results, we may conclude that the reaction probably involves two steps i.e. cleavage of Si-O bond in presence of F⁻ ion followed by cyclization and both steps are very fast and irreversible. It is assumed that deprotection of OTBS groups in derivative **8** provide optimum electron density for cyclization. The cyclization is also enthalpically favoured by greater conjugation of supertriphenylene relative to triphenylene. A feasible mechanism for this cyclization involves a common phenolate anion intermediate obtained via fluoride-mediated desilylation, followed by cyclization to supertriphenylene through oxidative dehydrogenation as shown in **Figure 6**.

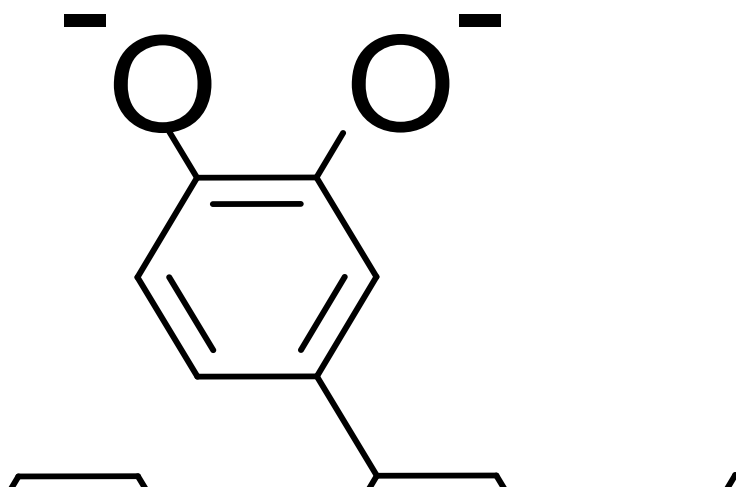


Figure 6: Proposed mechanism for fluoride induced cyclization of triphenylene to supertriphenylene.

We believe that the atmospheric oxygen is responsible for oxidative cyclization as deprotection reaction of **8** using tetrabutylammonium fluoride (TBAF) in THF followed by reaction with triflic anhydride proceeded well under oxygen atmosphere and derivative **8** was obtained in 72% yield. The drastic color change accompanying the deprotection reaction of compound **8** with TBAF prompted us to examine this reaction using UV-Vis. and fluorescence spectroscopy. The UV-Vis. experiments were carried out in THF at 1×10^{-5} M concentration of compound **8**. In the absence of F⁻ ions, the compound **8** shows absorption band at 306 nm which undergoes red shift to 325 nm ($\Delta\lambda$ 19 nm) upon the addition of 15 equiv. of F⁻ ions. At such low concentration, these changes were clearly visible to naked eye in which color of solution changed from colorless to green (**Figure 7a, inset**). However, there was no change in the absorption spectra of **8** upon the addition of other anions such as Cl⁻, Br⁻, I⁻, CN⁻, AcO⁻, NO₃⁻, H₂PO₄⁻, HSO₄⁻, OH⁻ and ClO₄⁻ (**Figure 7b**). We also used the fluorescence spectroscopy to investigate the behavior of **8** in the presence of F⁻ ions.

Interestingly, THF (1.0×10^{-6} M) solution of derivative **8** exhibits strong emission at λ_{\max} 395 nm and complete quenching of the emission band is observed upon addition of 12 μ M of F^- ions (**Figure 8**) and this quenching of the fluorescence was clearly visible to the naked eye under the illumination of UV light of 365 nm (**Inset, figure 8**). However with other anions no significant quenching in the emission intensity was observed (**Figure 9**). The complete fluorescence quenching may be ascribed to an electron transfer from phenolate oxygen to triphenylene moiety. It was found that **8** has a detection limit of 8×10^{-7} mol L^{-1} for F^- which is sufficiently low for the detection of submillimolar concentration range of F^- ions found in many chemical systems. To test the practical applicability of compound **8** as F^- selective sensor, competitive experiments were carried out in the presence of F^- at 12 μ M mixed with

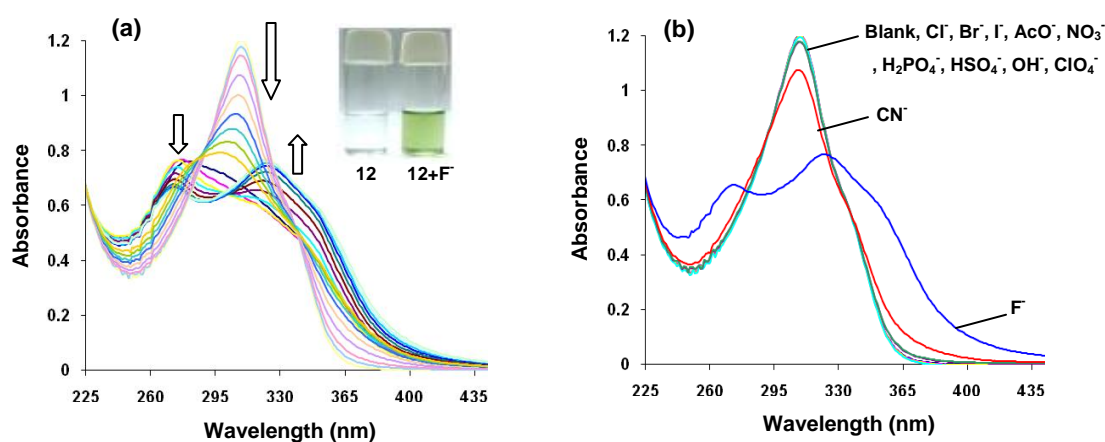


Figure 7: (a) The UV-Vis. spectra of **8** (1×10^{-6} M) upon the addition of F^- ions (15 equiv.) in THF. (b) The UV-Vis. spectra of **8** after the addition of 15 equiv. F^- , Cl^- , Br^- , I^- , CN^- , AcO^- , NO_3^- , $H_2PO_4^-$, HSO_4^- , OH^- , ClO_4^- in THF as solvent.

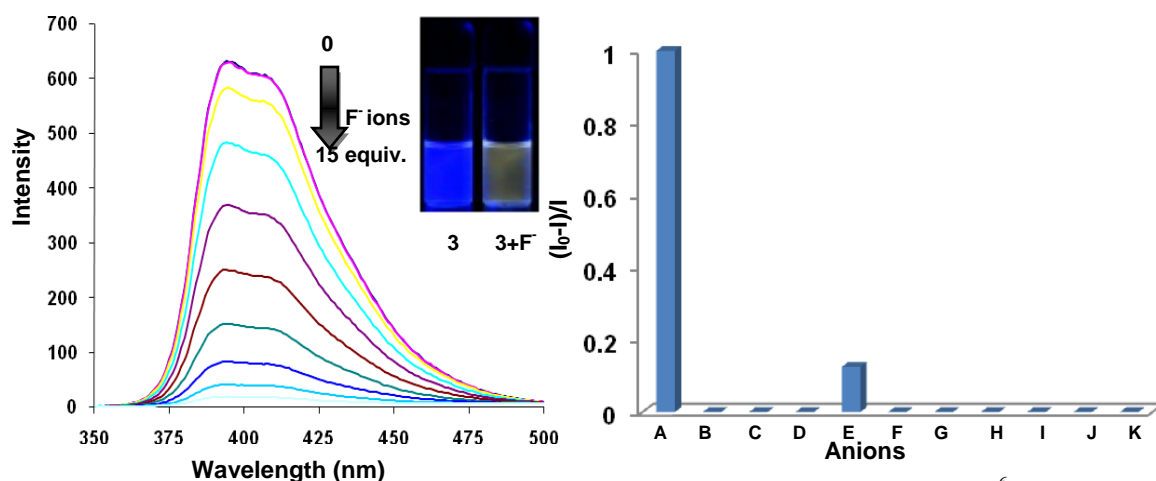


Figure 8: The fluorescence quenching of **8** (1×10^{-6} M) upon the addition of incremental amount of TBAF (0-15 equiv.) in THF. The inset shows fluorescence quenching upon the addition F^- ions.

Figure 9: Selectivity of **8** (1×10^{-6} M) toward F^- ions in the presence of other anions in THF. (A= F^- , B= Cl^- , C= Br^- , D= I^- , E= CN^- , F= HSO_4^- , G= $H_2PO_4^-$, H= NO_3^- , I= OAc^- , J= OH^- , K= ClO_4^-).

Cl⁻, Br⁻, I⁻, OAc⁻, HSO₄⁻, NO₃⁻, H₂PO₄⁻, CN⁻ at 200 μM, no significant variation in fluorescence behavior was observed by comparison with or without the other anions besides F⁻ (**Figure 10**). To check the practical applicability of compound **8** for detection of fluoride in water, we prepared a TLC strip by immersing it in the solution of **8** in THF. When exposed to 365 nm UV light illumination TLC strip shows blue fluorescence which switches off irreversibly when it was immersed in aqueous potassium fluoride solution (**Figure 11a**). Further, after drying it in air, the strip was then immersed in aqueous solution of potassium fluoride, an instant colorimetric change was observed which indicates sensing of fluoride ions (**Figure 11b**). Thus, this fluorescent switching can be used for instant detection of fluoride ions in aqueous media.

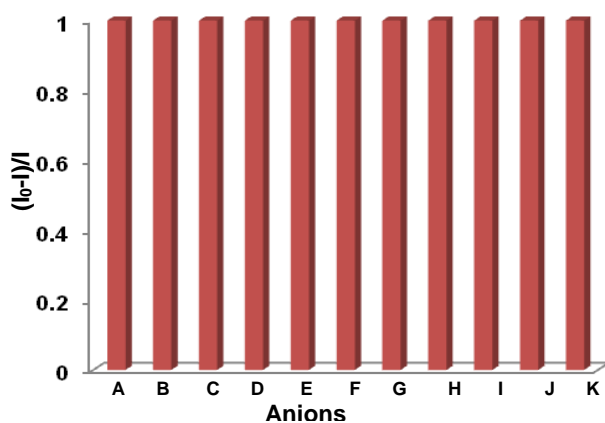


Figure 10: Competitive Selectivity of **8** (1×10^{-6} M) toward F⁻ ions in the presence of other anions in THF. (A=F⁻, B=Cl⁻, C=Br⁻, D= I⁻, E=CN⁻, F=HSO₄⁻, G=H₂PO₄⁻, H=NO₃⁻, I=OAc⁻, J=OH⁻, K= ClO₄⁻).

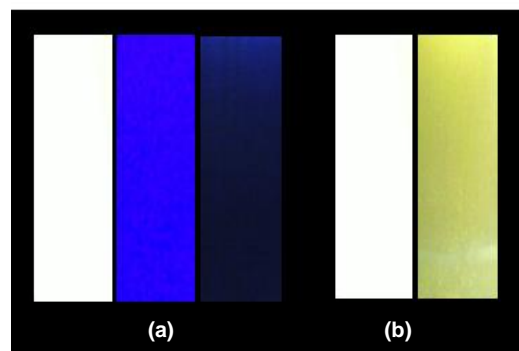


Figure 11: Naked eye detection of fluoride ions by compound **8** (a) fluorescence quenching and (b) colorimetric change after dipping the silica coated TLC strips in aqueous solution of KF.

In conclusion, triphenylene derivative **8** have been synthesized by Suzuki-Miyaura cross coupling in good yield which undergoes fluoride induced irreversible cyclization to form symmetrically substituted supertriphenylene derivative **9**. In addition, present study demonstrates the utility of TLC strip coated with derivative **8** for instant detection of fluoride ions in aqueous media.

(ii) Aggregates of triphenylene based chemosensing ensemble for sensitive detection of cyanide ions in aqueous medium

In the next part of the work, we were interested in the synthesis of triphenylene derivative which could undergo self-assembly in presence of metal ions. Further, we planned to utilize this self-assembled supramolecular architect for the detection of biologically important anions. Thus, we designed and synthesized star shaped triphenylene derivative having pyridine moieties which forms H-aggregates in presence of Cu²⁺ ions and this metal

coordination induced molecular aggregates of **11** works as selective ‘turn-on’ chemosensor for the CN⁻ ions.

Six fold Suzuki-Miyaura cross coupling of pyridine-3-boronic ester³ **10** with 2,3,6,7,10,11-hexabromotriphenylene **6** in 1,4-dioxane furnished the product **11** in 60% yield (**Scheme-3**). The structure of compound **11** was confirmed from its spectroscopic

Scheme 3

and analytical data. ¹H NMR spectrum of compound **11** in CDCl₃ showed two singlets at δ 8.64 (6H), 8.75 (6H), two doublets at 8.57 (6H) and 7.60 (6H) and one multiplet at 7.29 ppm (6H) due to the aromatic protons. The FAB mass spectrum showed a parent ion peak at 691(M⁺). These spectroscopic data corroborate the structure **11** for this compound. The presence of pyridine moieties in derivative **11** prompted us to evaluate its binding behaviour toward different metal ions using UV-vis and fluorescence spectroscopy. The titration experiments were carried out in EtOH: H₂O (8:2) by adding aliquots of different metal ions (Cu²⁺, Fe²⁺, Fe³⁺, Hg²⁺, Co²⁺, Pb²⁺, Zn²⁺, Ni²⁺, Cd²⁺, Ag⁺, Ba²⁺, Mg²⁺, K⁺, Na⁺, and Li⁺) as their perchlorate salts. The absorption spectrum of derivative **11**, (10 μM) showed an absorption band at 293 nm (**Figure 12**) in EtOH: H₂O (8:2). Upon addition of 150 equiv. of Cu²⁺ ions, the absorption band is blue shifted to 260 nm and level-off tail is observed in the visible region. The appearance of blue shifted band suggests the formation of H-aggregates of derivative **11** in presence of Cu²⁺ ions⁴. The scanning electron microscope (SEM) image of derivative **11** in EtOH: H₂O (8:2) shows presence of plate like aggregates (**Figure 13a**). However, on addition of copper ions, sponge like morphology is observed (**Figure 13b**). No significant change in absorption spectrum was observed in the presence of other metal ions such as Co²⁺, Fe²⁺, Pb²⁺, Hg²⁺, Zn²⁺, Ni²⁺, Cd²⁺, Ag⁺, Ba²⁺, Mg²⁺, K⁺, Na⁺, and Li⁺. The compound **11** showed strong blue fluorescence emission (φ= 0.35) at 386 nm in EtOH: H₂O (8:2) (**Figure 14**) when excited at 293 nm. Upon the addition of 50 equiv. of Cu²⁺ ions, quenching in the fluorescence emission was observed.

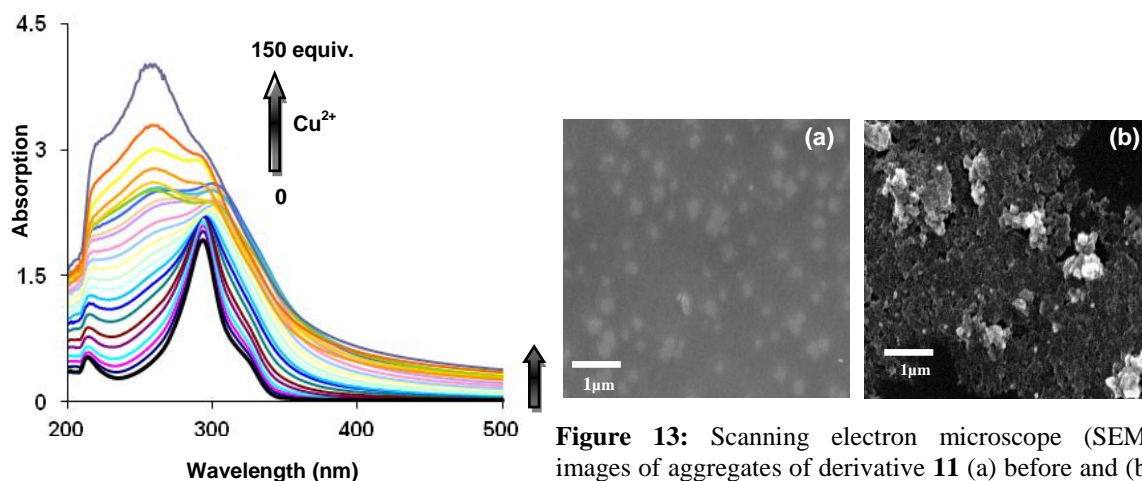


Figure 12: Absorption spectrum of derivative **11** (10 μM) on addition of Cu^{2+} ions (150 equiv.) in EtOH: H_2O (8:2) mixture buffered with HEPES (pH= 7.0).

Figure 13: Scanning electron microscope (SEM) images of aggregates of derivative **11** (a) before and (b) after the addition of Cu^{2+} ions in EtOH: H_2O (8:2) on glass substrate.

The fluorescence quenching of receptor **11** in the presence of Cu^{2+} ions attributed to the formation of non-fluorescent H-aggregates⁵ due to the face to face stacking of triphenylene moieties induced by the coordination of copper ions with nitrogen atoms of pyridine moieties, thus giving rise to sandwich like arrangement (**Scheme-4**). The Stern-Volmer plot shows that fluorescence intensity at 386 nm decreases with the increase in Cu^{2+} ion concentration (**Inset Figure 14**). This substantial decrease in the fluorescence emission of compound **11** in the presence of Cu^{2+} ions showed its credibility as a good Cu^{2+} sensor. Further, this quenching of the fluorescence was clearly visible to the naked eye under the illumination of UV light of 365 nm (**Inset figure 14**). Fitting the changes in the fluorescence spectra of compound **11**

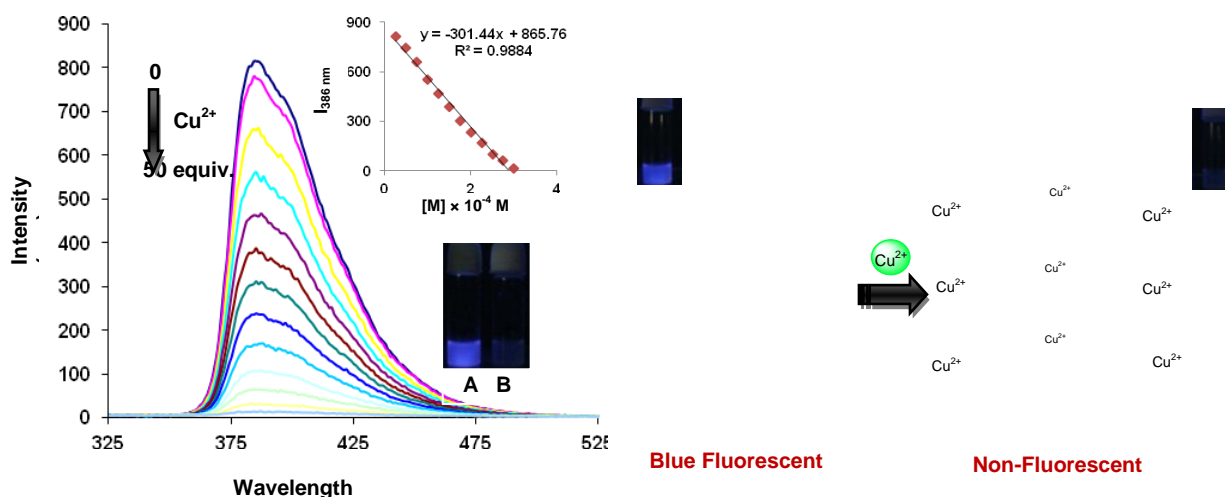


Figure 14: Fluorescence emission spectra of derivative **11** (5 μM) upon the addition of Cu^{2+} ions (0–50 equiv) in EtOH : H_2O (8:2) mixture buffered with HEPES (pH= 7.0). Inset shows the change in fluorescence intensity at 386 nm as the function of metal ion concentration and fluorescence images of **11** (1×10^{-4} M) (A) before (B) after the addition of Cu^{2+} ions.

Scheme 4: Proposed mechanism for fluorescence quenching of derivative **11** upon the addition of Cu^{2+} ions by the formation of face to face H aggregates.

with Cu^{2+} ions, using the nonlinear regression analysis program SPECFIT⁶ gave a good fit and demonstrated that 1:3 stoichiometry (host: guest) was the most stable species in the solution with a binding constant $\log \beta_{1,3} = 13.75$. The complex formation was further confirmed by ESI mass spectroscopy which shows a peak at $m/z = 1583$ corresponding to $\mathbf{11} + 3\text{Cu}(\text{ClO}_4)_2 + 6\text{H}_2\text{O}$ complex. Under the same conditions as used for Cu^{2+} ions, the (which show slight fluorescence quenching), no significant change in the fluorescence intensity was observed with other metal ions (**Figure 15**). To test the practical applicability of compound $\mathbf{11}$ as a Cu^{2+} selective fluorescence sensor, competitive experiments were carried out in the presence of Cu^{2+} ions at 50 equiv. mixed with other cations (Fe^{2+} , Cu^{2+} , Hg^{2+} , Ni^{2+} , fluorescence behaviour of $\mathbf{11}$ was tested with other metal ions (50 equiv.) such as Fe^{2+} , Zn^{2+} , Hg^{2+} , Ni^{2+} , Cd^{2+} , Pb^{2+} , Mn^{2+} , Co^{2+} , Li^+ , Na^+ , Mg^{2+} , K^+ , Ca^{2+} , Ba^{2+} ions, apart from Hg^{2+} , Cd^{2+} , Pb^{2+} , Mn^{2+} , Co^{2+} , Li^+ , Na^+ , Mg^{2+} , K^+ , Ca^{2+} , Ba^{2+}), at 200 equiv., no significant variation was found by comparison with and without the other metal ions (**Figure 16**). The detection limit of $\mathbf{11}$ as a fluorescent sensor for the analysis of Cu^{2+} was found to be 1.5×10^{-6} M. The well-known interaction between copper and cyanide ions prompted us to evaluate the binding behaviour of $\mathbf{11} \cdot \text{Cu}^{2+}$ ensemble toward various anions such as CN^- , OAc^- , NO_3^- , F^- , Cl^- , Br^- , I^- , HSO_4^- , SO_3^{2-} , S^{2-} , N_3^- , ClO_4^- . Complete revival of fluorescence emission of the $\mathbf{11} \cdot \text{Cu}^{2+}$ ensemble was observed upon the addition of 300 equiv. of CN^- ions (**Figure 17**). This revival in the fluorescence intensity may be ascribed to strong interactions between Cu^{2+} ions and CN^- ions and formation of stable $[\text{Cu}(\text{CN})_x]^{n-}$ complex which results in the deaggregation of $\mathbf{11} \cdot \text{Cu}^{2+}$ ensemble (**Figure 19**). This turn on sensing of CN^- ion by $\mathbf{11} \cdot \text{Cu}^{2+}$ ensemble was clearly visible to the naked eye under the UV illumination of 365 nm (**Inset**

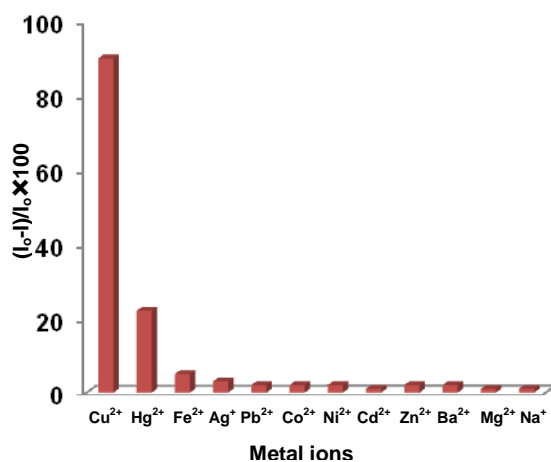


Figure 15: Selectivity of receptor $\mathbf{11}$ ($5 \mu\text{M}$) towards Cu^{2+} upon addition of different metal ions (50 equiv.) in EtOH: H_2O (8:2) mixture buffered with HEPES (pH = 7.0)

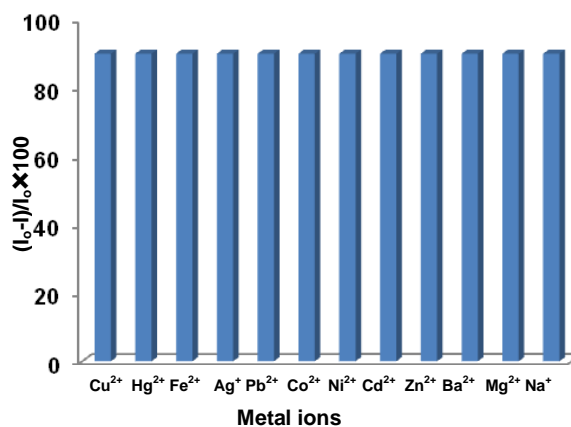


Figure 16: Competitive Selectivity of receptor $\mathbf{11}$ ($5 \mu\text{M}$) towards Cu^{2+} in the presence of other metal ions (200 equiv.) in EtOH: H_2O (8:2) mixture buffered with HEPES (pH = 7.0)

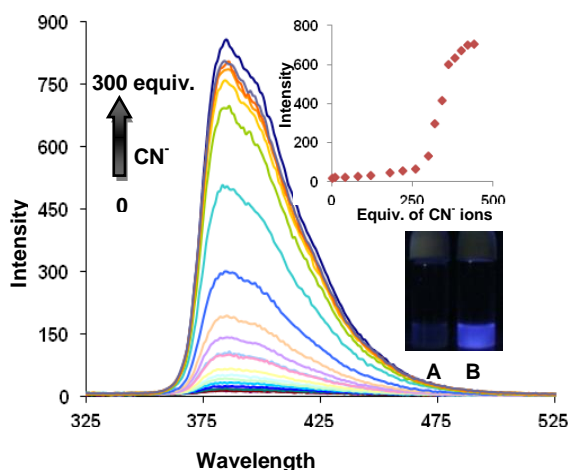


Figure 17: Fluorescence emission spectra of receptor $11.Cu^{2+}$ upon the addition of CN^- ions (0–300 equiv) in EtOH: H_2O (8:2) mixture buffered with HEPES (pH= 7.0). Inset shows the change in fluorescence intensity at 386 nm as the function of equivalents of cyanide ions added and fluorescence images of (A) copper ensemble, $11.Cu^{2+}$ (1×10^{-4} M) (B) $15.Cu^{2+}$ + CN^- ions in EtOH: H_2O (8:2)

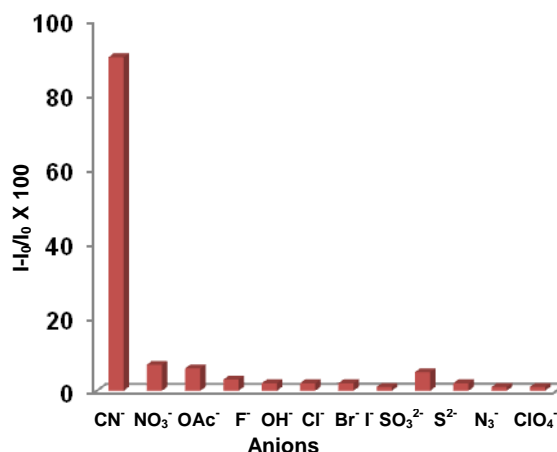


Figure 18: Selectivity of $11.Cu^{2+}$ towards CN^- upon addition of different anions (300 equiv.) in EtOH: H_2O (8:2) mixture buffered with HEPES (pH = 7.0)

figure 17). On the other hand, with other anions (300 equiv.) such as OAc^- , NO_3^- , F^- , Cl^- , Br^- , I^- , HSO_4^- , SO_3^{2-} , S^{2-} , N_3^- , ClO_4^- no significant enhancement in fluorescence intensity was observed (**Figure 18**). To performed competitive experiments in the presence of CN^- (300 equiv.) mixed with other anions (800 equiv.) such as OAc^- , NO_3^- , F^- , Cl^- , Br^- , I^- , HSO_4^- , SO_3^{2-} , S^{2-} , N_3^- , ClO_4^- and no check the practical applicability of aggregates of $11.Cu^{2+}$ ensemble as cyanide sensor, we significant change in fluorescence intensity was observed by comparison with and without other anions (**Figure 20**). The detection limit of CN^- ions was determined to be as low as 0.026 ppm which is much lower than the maximum limit (0.2 ppm) of cyanide in the drinking water as set by the U.S. environment protecting agency. For trace detection of cyanide ions in tap water, we carried out the fluorescence titration of $11.Cu^{2+}$ ensemble with

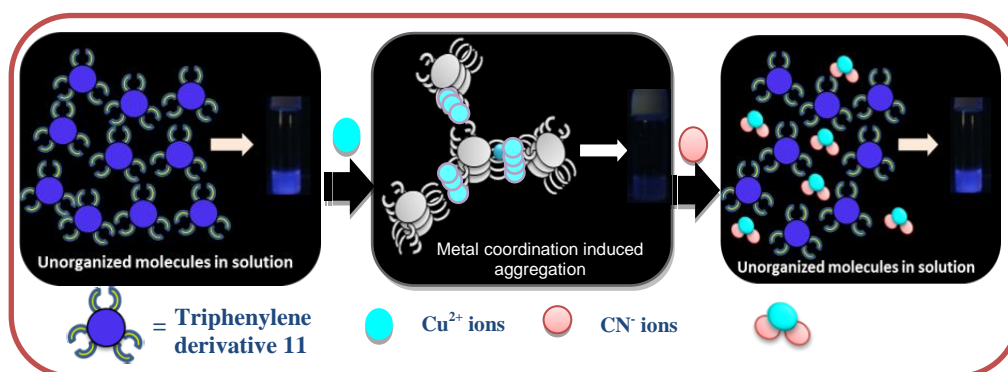


Figure 19: Pictorial picture showing the ‘Turn-ON’ sensing of CN^- ions with the nanoaggregates of copper ensemble of triphenylene derivative **11**.

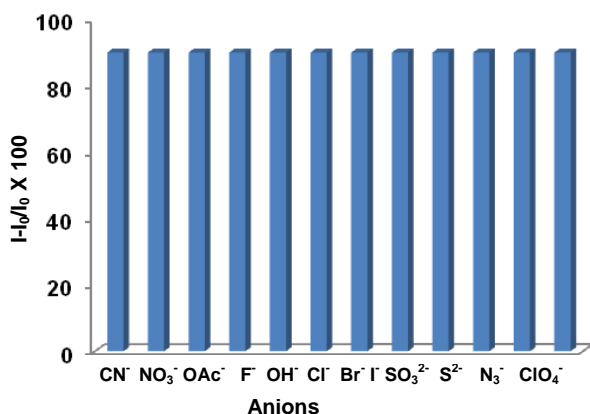


Figure 20: Competitive Selectivity of **11.Cu²⁺** towards **CN⁻** over other anions (300 equiv.) in EtOH: H₂O (8:2) mixture buffered with HEPES (pH = 7.0)

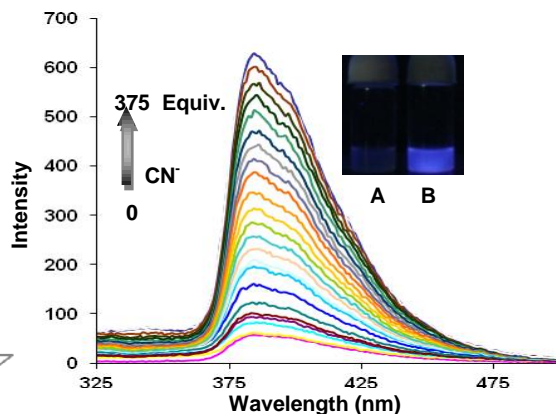


Figure 21: Fluorescence emission spectra of receptor **11.Cu²⁺** (5μM) upon the addition of **CN⁻** ions (0–375 equiv) in EtOH: H₂O (8:2; buffered with HEPES pH=7.4) in the presence of blood serum. Inset, fluorescence images of (A) **11.Cu²⁺** (B) upon the addition of **CN⁻** ions.

tap water spiked by NaCN and similar fluorescence results were obtained. The detection limit of inorganic **CN⁻** ions (NaCN) in tap water was found to be 0.1 ppm which is under the EPA regulations. The ability of **11.Cu²⁺** ensemble to detect the cyanide in biological medium was tested by carrying out the fluorescence titration with cyanide in the presence of blood serum milieu⁷. Almost negligible change was observed in the fluorescence intensity of the **11.Cu²⁺** upon addition of blood serum and revival in the fluorescence was observed upon the addition of 375 equiv. of **CN⁻** ions (**Figure 21**). The practical application of **11.Cu²⁺** ensemble for the detection of **CN⁻** ions was realized by using solution coated silica strip. The solution coated strips of derivative **11** showed blue emission under UV illumination of 365 nm. After drying in air, the strip was immersed in the aqueous solution of **Cu(ClO₄)₂** and the blue fluorescence

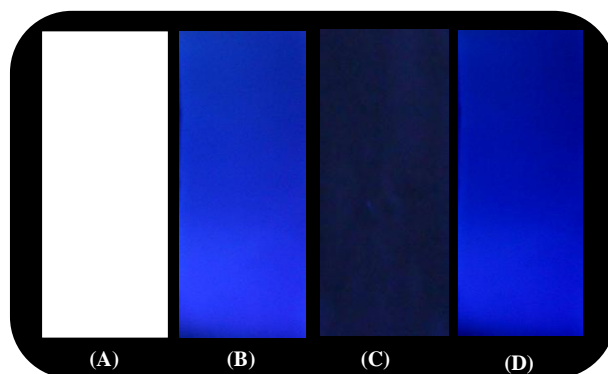


Figure 22: Naked eye and solid state detection of **Cu²⁺** ions with silica coated TLC strips. (a) only test strip (b) test strip coated with **11**, excited at 365 nm using UV light (c) after dipping the coated strip in solution containing **Cu(ClO₄)₂** (d) after dipping the coated strip c in aqueous solution of NaCN.

of derivative **11** completely quenched. However, the quenched fluorescence again revived upon dipping this test strip in the aqueous solution of NaCN (**Figure 22**).

In conclusion, we designed and synthesized star shaped highly fluorescent triphenylene derivative **11** which forms nanoaggregates in presence of Cu^{2+} ions in mixed aqueous medium by the metal induced face to face stacking of molecules. Interestingly, among various anions tested, aggregates of copper ensemble of derivative **11**, dissociates upon the addition of CN^- ions by the coordination complex displacement approach, thereby reviving the fluorescence of the ensemble. The **11.Cu²⁺** ensemble can also detect inorganic cyanide ions in the tap water. Further, the solution coated strip of **11.Cu²⁺** ensemble was used for detection of CN^- ions in aqueous medium.

(iii) Carbazole Substituted Triphenylene Derivative for the Sensitive Detection of Nitroaromatic Explosives

Explosives are major threat to the mankind and international peace. The large scale use of these explosives by the terrorist groups prompted the scientific community to develop the novel sensing materials for their detection. Keeping this in view, we designed and synthesized derivative **13** having electron rich triphenylene as the core moiety. Apart from this triazole modified triphenylene derivative **19** also act as potent chemosensors for nitroaromatic explosives. Triphenylene derivative **13** having carbazole moieties has extended conjugation but no tendency to undergo aggregation whereas derivative **19** having triazole moieties, forms supramolecular aggregates in solution.

Triphenylene derivative **13** having carbazole groups was prepared using Suzuki-Miyaura coupling protocol (**Scheme 5**) while derivative **19** was obtained by 'click reaction' of precursor **18**^{15a} with dodecyl-azide in the presence of CuI in 52% yield

Scheme 5

(Scheme 6). Suzuki-Miyaura coupling of 9-hexyl-9H-carbazole-3-ylboronic acid⁸ **12** with 2,3,6,7,10,11-hexabromotriphenylene⁹ **6** furnished compound **13** in 50 % yield. (Scheme 6). ¹H NMR spectrum of derivative **13** showed two triplets at 0.82 (18H -CH₃) and 4.20 (12H -NCH₂), two multiplets at 1.22-1.33 (36H -CH₂), 1.77-1.82 (12H -CH₂) corresponding to the protons of hexyl chain, two multiplets at 7.09-7.17 (12H), 7.32-7.39 (18H), two doublets (6H each) at 8.02, 8.29 and a singlet at 8.99 (6H) ppm corresponding to the aromatic protons. The structure of compound **13** was further confirmed by MALDI-TOF mass spectrum which showed a parent ion peak at m/z 1723 (M)⁺. These spectroscopic data corroborate the structure **13** for this compound. The presence of carbazole moieties in derivative **13** not only enhances the conjugation but also prevents the intermolecular π - π stacking due to its bulky size which is responsible for its high emission intensity ($\phi = 0.50$) in mixed aqueous media. On the other hand, triphenylene derivative **19** forms stable organogel in cyclohexane and mixed solvents such as hexane and dichloromethane (1:4, v/v) (Figure 23). Further, due to the greater tendency of derivative **19** to undergo aggregation in non-polar

Scheme 6

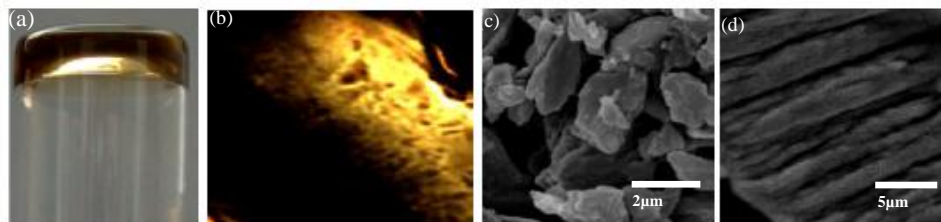


Figure 23: The photograph of (a) gel of compound **19** (1.6 % w/v) formed in cyclohexane (b) polarized optical micrographs of compound **19** through crossed polarizing filters (magnification $\times 50$) (c-d) Scanning electron micrographs of gel of derivative **19** in cyclohexane.

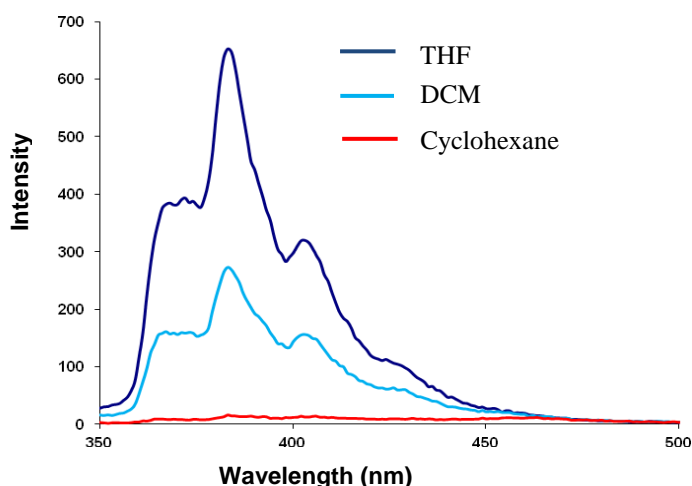


Figure 24: Fluorescence emission spectra of derivative **19** in solvents of different polarity.

solvent, its solution in cyclohexane is non-emissive (**Figure 24**). However, in the polar solvents such as tetrahydrofuran (THF), less aggregation tendency is observed due to the weak π - π interactions between the molecules. This is evident from good emission intensity of derivative **19** ($\phi = 0.22$) in solvent mixture of THF: H_2O (9.5:0.5, v/v).

The electrochemical properties of the compounds **13** and **19** were evaluated with the help of cyclic voltammetry (**Figure 25**). Taking -4.8 eV as the highest occupied molecular orbital (HOMO) energy level for the ferrocene/ferrocenium redox system¹⁰,

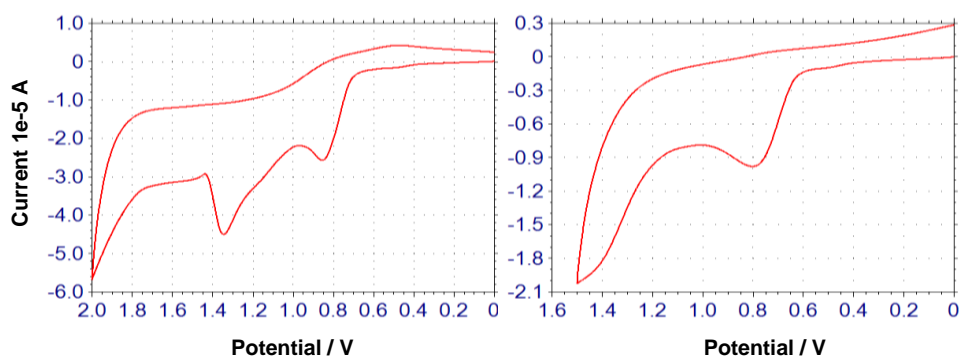


Figure 25: Cyclic voltammogram of derivative (A) **13** and (B) **19** (1×10^{-3} M) in dichloromethane (DCM).

HOMO energy level of -5.65 eV and -5.60 eV were calculated for **13** and **19**, respectively. These values indicate that the compounds **13** and **19** are highly electron rich. The electrochemical studies and reasonably good emission intensity of derivative **13** and **19** in THF: H₂O (9.5:0.5) mixture prompted us to explore the potential applications of these derivatives as chemosensor for the detection of nitroaromatics such as picric acid (PA), 2,4,6-trinitrotoluene (TNT), 2,4-dinitrotoluene (DNT), 1,4-dinitrobenzene (DNB), 4-nitrotoluene (4-NT), 1,4-benzoquinone (BQ), nitromethane (NM) and 2,3-dimethyl-2,3-dinitrobutane (DMNB). Thus, we carried out the fluorescence titrations of these compounds (5 μM) toward various nitroaromatic derivatives in THF: H₂O (9.5:0.5) mixture. Derivative **13** showed fluorescence emission at 410 nm when excited at 305 nm. However, upon the incremental addition of picric acid (0 to 50 equiv.), there is a quenching of fluorescence in the emission spectrum of **13** (**Figure 26**) and this quenching of the fluorescence was clearly visible to the naked eye under the illumination of UVlight of 365 nm (**Inset, figure 26**). The observed quenching of fluorescence is attributed to the energy transfer from photo-excited π-electron rich

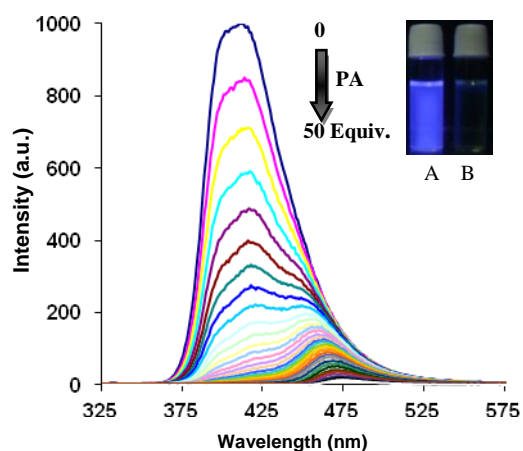


Figure 26: Fluorescence emission spectra of receptor **13** (5 μM) upon the addition of PA (0–50 equiv.) in THF: H₂O (9.5:0.5) mixture. Inset shows the fluorescence of derivative **13**, before (A) and after (B) the addition of picric acid.

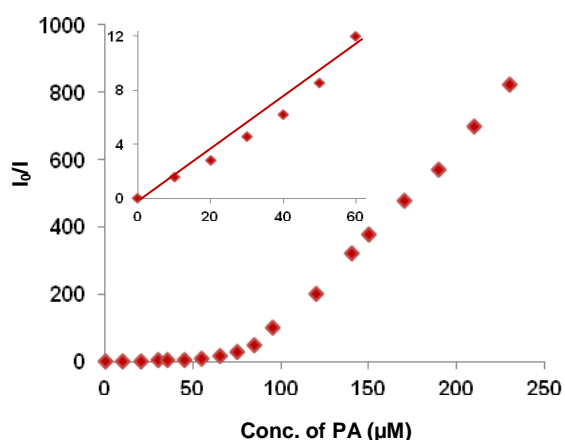


Figure 27: Stern-Volmer plot for the quenching of fluorescence of derivative **13** with PA upon the addition of 50 equiv. of PA. Inset shows the Stern-Volmer plot at lower conc. (upto 12 equiv.)

derivatives **13** to ground state electron deficient picric acid which was further confirmed by the spectral overlap of the emission spectrum of derivative **13** with the absorption spectrum of picric acid (**Figure 28, 29**; respectively). The detection limit of derivative **13** for picric acid was found to be 400 nM. The calculated Stern-Volmer constant (K_{sv}) was found to be $2.91 \times 10^5 \text{ M}^{-1}$ for PA. The Stern-Volmer plot was

found to be linear at lower concentration (upto 60 μM , **Inset Figure 27**) which indicates that fluorescence quenching involves the static quenching mechanism at lower concentration of nitroaromatic compound but at higher concentration the plot was found to be hyperbolic curved (**Figure 27**) which may be due to the combination of both static and dynamic (collision) quenching¹¹. On addition of compounds such as 4-NT (85 equiv.), DNB (200 equiv.), DNT (260 equiv.), TNT (300equiv.), complete quenching in the emission spectrum was observed. However with other electron deficient compound such as BQ 1500 equivalents were required to various electron deficient nitroaromatic completely quench the fluorescence while with BA and DMNB a slight quenching was observed even after the addition of 1500 equivalents. The relative fluorescence quenching ability of various nitroaromatic compounds towards the derivative **13** is summarised in the bar diagram (**Figure 30**) by taking the picric acid as reference which shows complete quenching at 50 equiv. of its addition. Under similar set of conditions, derivative **19** showed emission at 384 nm ($\lambda_{\text{ex}}=275$ nm), which quenched upon the addition of 30 equiv. of PA (**Figure 32**) and this quenching of the fluorescence was also clearly visible to the naked eye under the illumination of

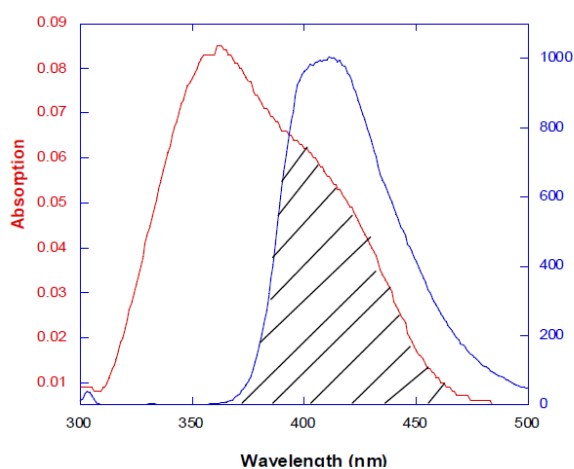


Figure 28: Spectral overlap of the absorption spectrum of picric acid (red line) with the emission spectrum of compound **13** (blue line).

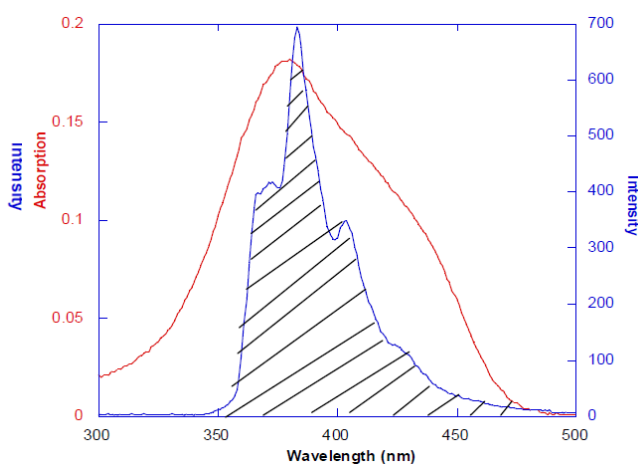


Figure 29: Spectral overlap of the absorption spectrum of picric acid (red line) with the emission spectrum of compound **19** (blue line).

UV light of 365 nm (**inset figure 32**). A hyperbolic curved Stern-Volmer plot was obtained obtained upon plotting the concentration of PA added and change in the fluorescence intensity (**Figure 33**) which was also found to be linear at lower concentration (upto 30 μM , **inset figure 33**). Detection limit of 50 nM and a Stern-Volmer constant (K_{sv}) of $2.93 \times 10^5 \text{ M}^{-1}$ was calculated for PA. The complete quenching in the fluorescence intensity was also observed by the use of much higher

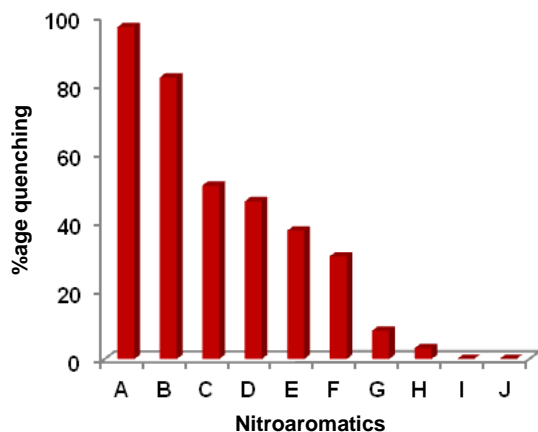


Figure 30: Bar diagram showing the percentage quenching of fluorescence of derivative **13** (5 μM) upon the addition of 50 equiv. of various nitroaromatics (A = Picric acid, B = 4-nitrotoluene, C = 1,4-dinitrobenzene, D = 2,4-dinitrotoluene, E = 2,4,6-trinitrotoluene, F = 4-nitrobenzene, G = 1,4-benzoquinone, H = 2,3-dimethyl-2,3-dinitrobutane, I = benzoic acid, J = nitromethane).

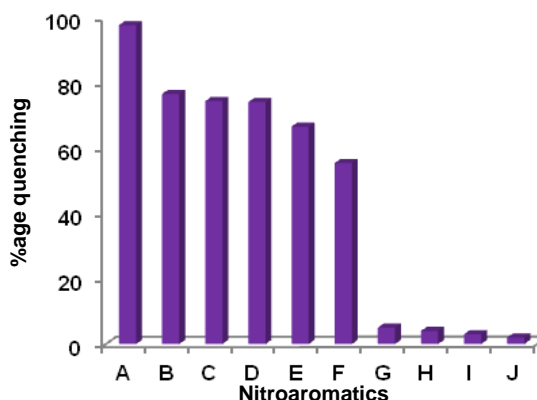


Figure 31: Bar diagram showing the percentage quenching of fluorescence of derivative **19** (5 μM) upon the addition of 50 equiv. of various nitroaromatics (A = Picric acid, B = 2,4-dinitrotoluene, C = 4-nitrotoluene, D = 1,4-dinitrobenzene, E = 4-nitrobenzene, F = 2,4,6-trinitrotoluene, G = 1,4-benzoquinone, H = benzoic acid, I = 2,3-dimethyl-2,3-dinitrobutane, J = nitromethane).

concentration of other nitroaromatic compounds such as 4-NT (75 equiv.), DNB (80 equiv.), DNT (110 equiv.), TNT (140 equiv.), NB (135 equiv.) and bar diagram was constructed similarly as in the case of derivative **20** (**Figure 31**). These results indicate that although derivative **13** shows high emission intensity but derivative **19** exhibits more sensitive response towards nitroaromatics. We assume that strong spectral overlap observed in case of derivative **19** is responsible for its high sensitivity towards picric acid. Further, we believe that though derivative **19** does not form gel in

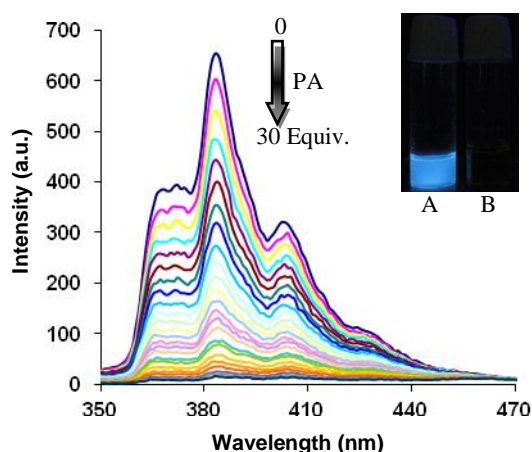


Figure 32: Fluorescence emission spectra of receptor **23** (5 μM) upon the addition of PA (0–30 equiv) in THF:H₂O (9.5:0.5) mixture. Inset shows the fluorescence quenching of derivative **19**, before (A) and after (B) the addition of picric acid.

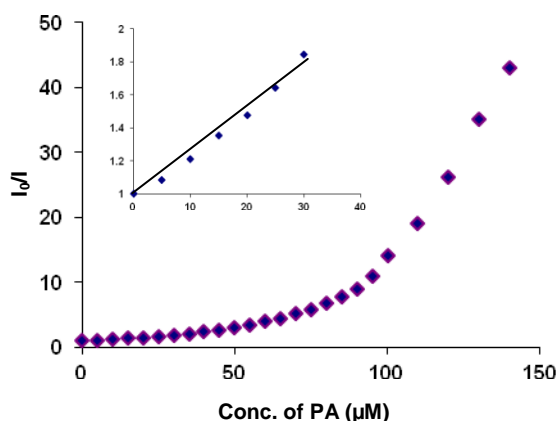


Figure 33: Stern- Volmer plot for the quenching of fluorescence of derivative **19** with PA upon the addition of 30 equiv. of PA. Inset shows the Stern- Volmer plot at lower conc. (upto 6 equiv.) of PA.

the solvent mixture of THF: H₂O (9.5:0.5) due to the weak π - π interactions between the molecules yet its molecules have ordered organisation as compared to that of derivative **13** thus, enabling long range exciton migration and their quick annihilation by the explosive quenchers¹².

We prepared the test strips by dip coating the THF solution of derivative **13** and hot gel solution of derivative **19** on TLC strip followed by drying the strips under vacuum.

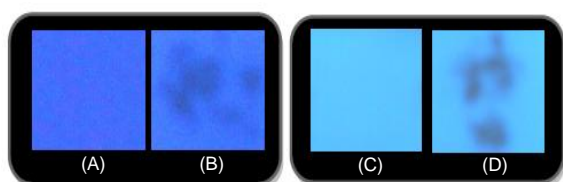


Figure 34: Contact mode detection of picric by derivative **13** (A and B) and **19** (C and D) under UV light illumination on TLC Strips after in contact with PA for 5 seconds. [The size of each test strip is 1cm²].

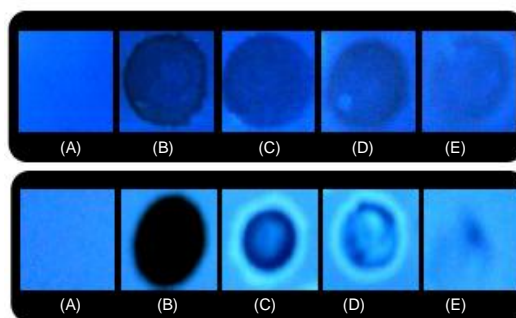


Figure 35: Photographs of fluorescence quenching (under 365 nm UV light) of solution coated strips of compound **17** (upper row) and gel coated strips of compound **19** (lower row) for the visual detection of small amount of PA (A) test strip with a drop of water ; PA of different concentration (B) 10⁻³ M (C) 10⁻⁵ M (D) 10⁻⁷ M (E) 10⁻⁹ M. [The size of each test strip is 1cm²].

PA crystals were placed over a test strip for 5 sec. To test the contact mode response, upon illumination with UV lamp, black spots were observed in the contact area (**Figure 34**). For detection of very small amounts of PA, we prepared the aqueous solution of PA of different concentration and 6 μ L of each solution was placed on the solution coated strips of derivative **13** and gel coated test strips of derivative **19**, respectively (**Figure 34**). The minimum amount of PA, detectable by naked eye was upto 14pg/cm².

In conclusion, we designed and synthesized π -electron rich triphenylene derivatives **13** and **20** which act as efficient sensors for trace detection of various nitroaromatics such as PA, TNT and DNT which are major constituents of most of the explosives. Derivative **13** having carbazole moieties exhibit high emission intensity due to extended conjugation. Despite high emission intensity of derivative **13**, derivative **19** exhibits more sensitive response toward nitroaromatic derivatives which may be attributed to the ordered organization of derivative **19**. Further, the present study shows the utility of low cost and portable gel coated paper strips of derivative **19** for

detection of picric acid in contact mode and aqueous media with a detection limit in the range of 14 pg/cm².

(iv) Fluorescent Aggregates of AIEE active Triphenylene Derivatives for the Sensitive Detection of Picric Acid

Triphenylene derivative **21** was synthesized by six fold Suzuki-Miyaura coupling of 4-cyanophenyl boronic ester **20**¹³ with 2,3,6,7,10,11- hexabromo triphenylene **6** (**Scheme 4**). The structure of derivative **21** was confirmed from its spectroscopic and analytical data. The ¹H NMR spectrum of derivative **21** showed two doublets (12H each) at 7.40 and 7.64 ppm and a singlet (6H) at 8.68 ppm corresponding to aromatic protons. The MALDI- TOF mass spectrum of derivative **21** showed a peak at m/z 834.163 (M⁺). These spectroscopic data corroborates the structure **21** for this compound.

Scheme 7: Synthesis of triphenylene derivative 21

Derivative **21** having electron withdrawing nitrile groups shows absorption band at 306 nm in pure THF (**Figure 36**), however, on increasing the water fraction from 0 to 70 %, it undergoes red shift of 12 nm along with ‘leveling of tail’ in the visible region. The leveling of tail indicates the formation of aggregates. The fluorescence spectrum of derivative **21** exhibits an emission band at 393 nm ($\Phi = 0.29$). Upon increasing the water fraction from 0 to 50%, 1.5 folds enhancement ($\Phi = 0.44$) in the emission signal was observed (**Figure 37 A**). Further increase in the water fraction from 60 to 90 % resulted in the red shifting and broadening of emission band along with the decrease in emission intensity. The observed behaviour is due to the presence of electron deficient cyano groups at the periphery of triphenylene which make it a donor-acceptor system and such type of donor-acceptor systems tend to adopt twisted conformation in more polar solvents which exhibits twisted intramolecular charge transfer (TICT) in excited state susceptible to various non-radiative quenching processes.¹⁴ The SEM image of derivative **21** in H₂O: THF (1:1) mixture showed flake like morphology of aggregates (**Figure 37 B**).

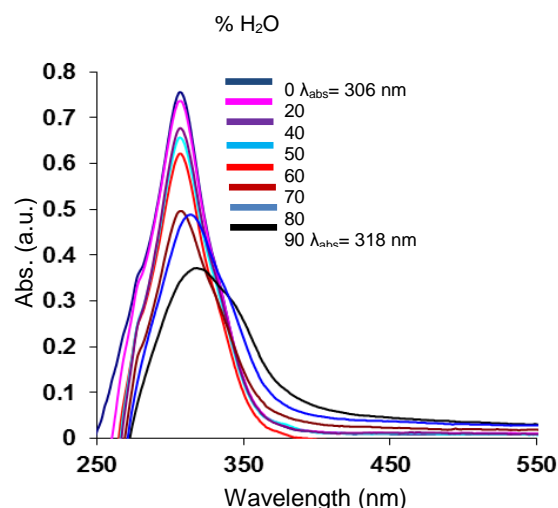


Figure 36: UV-vis. spectra of derivative **21** (10 μ M) showing the variation of absorption intensity in THF/H₂O mixture with different water fractions.

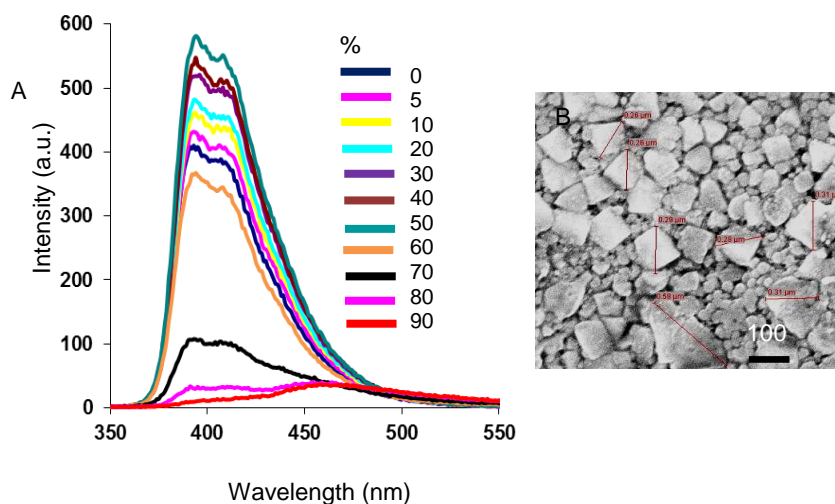


Figure 37: (A) Fluorescence emission spectra of derivative **21** (10 μ M) in different fraction of water in THF (B) SEM image of derivative **21** in H₂O:THF (1:1) mixture. Scale bar 100 nm.

On the basis of absorption and fluorescence studies, we believe that molecules of derivative **21** are packed in slipped face to face fashion in aggregated state¹⁵ and formation of non-fluorescent H-aggregates is restricted. The dynamic light scattering (DLS) studies shows that average diameter of aggregates of derivative **21** increases from 350 to 580 nm upon increasing the water fraction from 30% to 50% respectively (**Figure 38**). Thus enhancement of emission signal is related to the aggregation driven growth of the aggregates¹⁶ and a linear relationship between emission enhancement and size of aggregates of derivative **21** is observed (**Inset; Figure 38**).

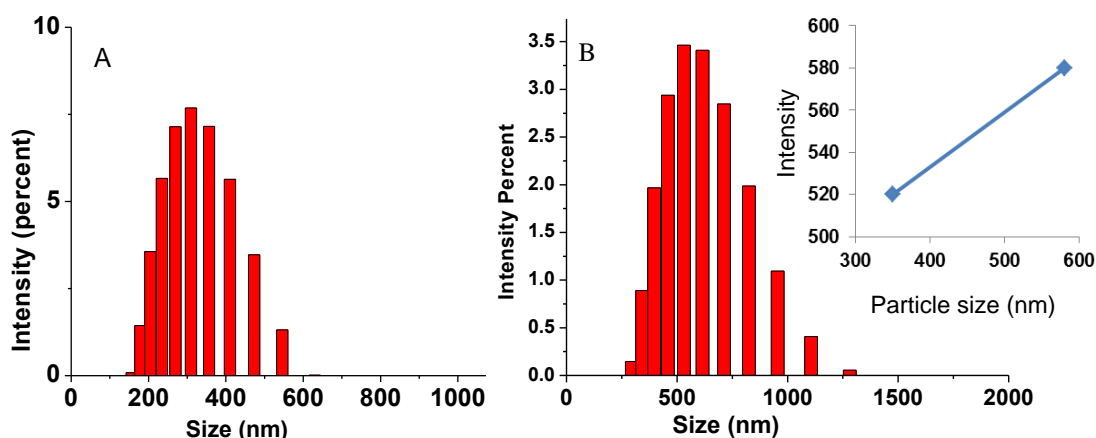


Figure 38: Dynamic light scattering (DLS) measurements of solutions of derivative **21** ($10\ \mu\text{M}$) in different fractions of water in THF (A) $\text{H}_2\text{O}:\text{THF}$ (3:7) (B) $\text{H}_2\text{O}:\text{THF}$ (1:1). Inset shows the plot of emission intensity vs. particle size.

Further, to get insight into the mechanism of fluorescence enhancement in derivative **21**, we investigated the effect of increasing viscosity. For this, we carried out fluorescence studies of derivative **21** in different fractions of triethylene glycol (TEG) in THF. Upon the addition of 90% volume fraction of TEG to the THF solution of derivative **21**, fluorescence enhancement was observed (**Figure 39**). This enhancement suggests the restriction of rotation of the phenyl rotors with respect to rigid triphenylene core upon increasing the viscosity of

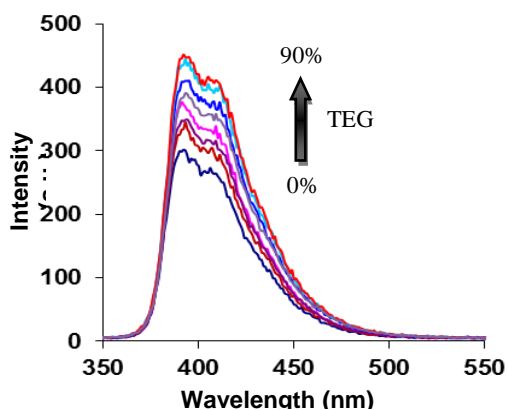


Figure 39: Effect of viscosity on the fluorescence emission spectra of derivative **21**.

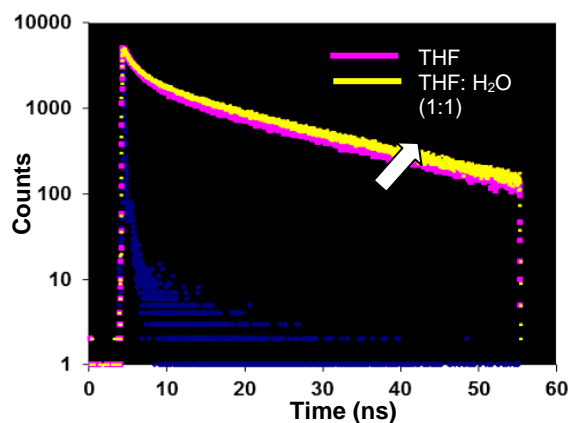


Figure 40: Time resolved fluorescence spectrum of derivative **21** ($10\ \mu\text{M}$) in pure THF and $\text{H}_2\text{O}:\text{THF}$ (1:1) ($\lambda_{\text{ex}} = 377\text{nm}$).

the medium. These studies show that restriction to rotation (RIR) is one of the reasons for observed AIEE in derivatives **21**. We also carried out time resolved fluorescence studies of derivatives **21** to determine the fluorescence life times of derivative **21** in THF and in aggregated state (**Figure 40**, **Table 1**). The life time of derivatives **21** was higher in their

aggregated state as compared to their solution in THF. This increase in lifetime suggests the formation of ordered aggregates.¹⁷

Further to evaluate the effect of electronic nature of the substituents on the AIEE behaviour of triphenylene derivatives, we have studied the AIEE behaviour of derivative **16** having electron donating amino groups at the periphery. UV-vis absorption spectrum of derivative **22** in THF exhibits an absorption band at 322 nm (**Figure 41**). Upon addition of water (90% volume fraction) to the THF solution of derivative **22**, a broad absorption band along with leveling of tail is observed in the visible region. The appearance of a ‘*level-off*’ long wavelength tail may be attributed to the formation of aggregates. The fluorescence spectrum of derivative **22** showed emission at 428 nm in pure THF ($\Phi = 0.34$)¹⁸ when excited at 322 nm (**Figure 42**). Upon addition of water fractions up to 70%, fluorescence enhancement ($\Phi = 0.54$) was observed with the bathochromic shift of 30 nm. Further, addition of more than 70% water fraction to THF solution of derivative **22** resulted in decrease in fluorescence intensity. This phenomenon is often observed in derivatives with AIEE properties as after the aggregation only the molecules on the surface of aggregate emit light and contribute to the fluorescent intensity upon excitation and this leads to a decrease in emission intensity.¹⁹ The scanning electron microscope (SEM) analysis of derivative **22** in H₂O:THF (7:3) mixture shows the formation of irregular shaped aggregates (**Figure 43 A**).

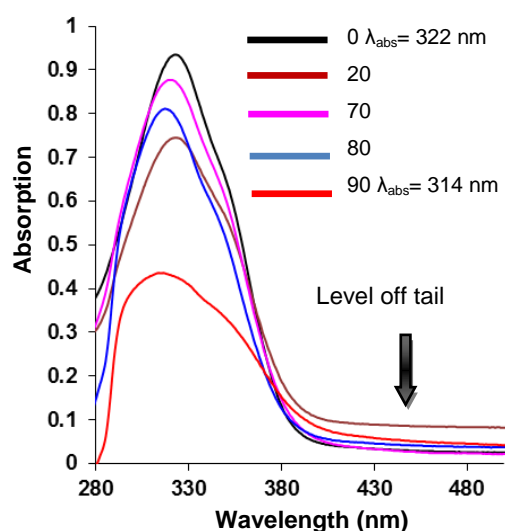


Figure 41: UV-vis. spectra of derivative **22** (10 μ M) showing the variation of absorption intensity in THF/H₂O mixture with different water fractions.

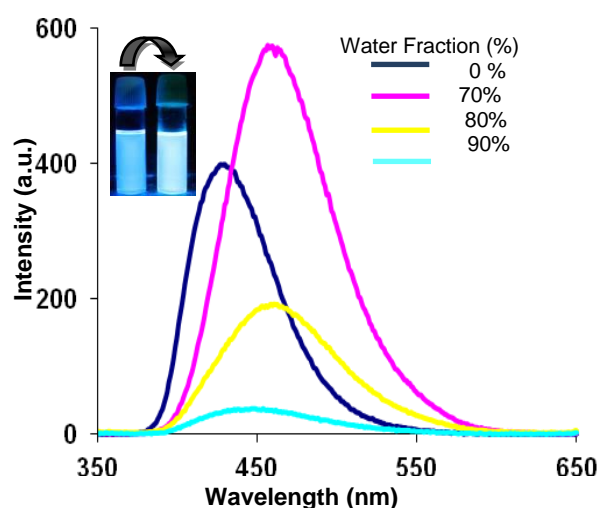


Figure 42: Fluorescence emission spectra of derivative **22** (10 μ M) in different fractions of H₂O in THF.

Confocal microscope image of derivative **22** in H₂O:THF mixture (7:3) also showed the presence of fluorescent aggregates (**Figure 43 B**). The dynamic light scattering (DLS) studies clearly showed average size of aggregates of derivative **22** around 210 nm, 615 nm and 1281 nm in 30%, 50%, and 70% H₂O/THF solvent mixture respectively (**Figure 44 A-C**). A linear relationship between emission enhancement and size of aggregates of derivative **20** was observed (**Figure 44 D**). Further, increase in the viscosity of the medium also resulted in the increase in emission intensity (**Figure 45**). The lifetime of derivative **22** in aggregated state was found to be higher than that in molecular state which suggests the formation of ordered aggregates (**Figure 46**).

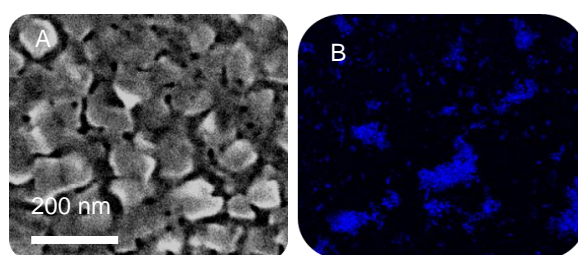


Figure 43: (A) Scanning electron microscope (SEM) and (B) Confocal fluorescence microscope image of derivative **22** in H₂O:THF mixture (7:3).

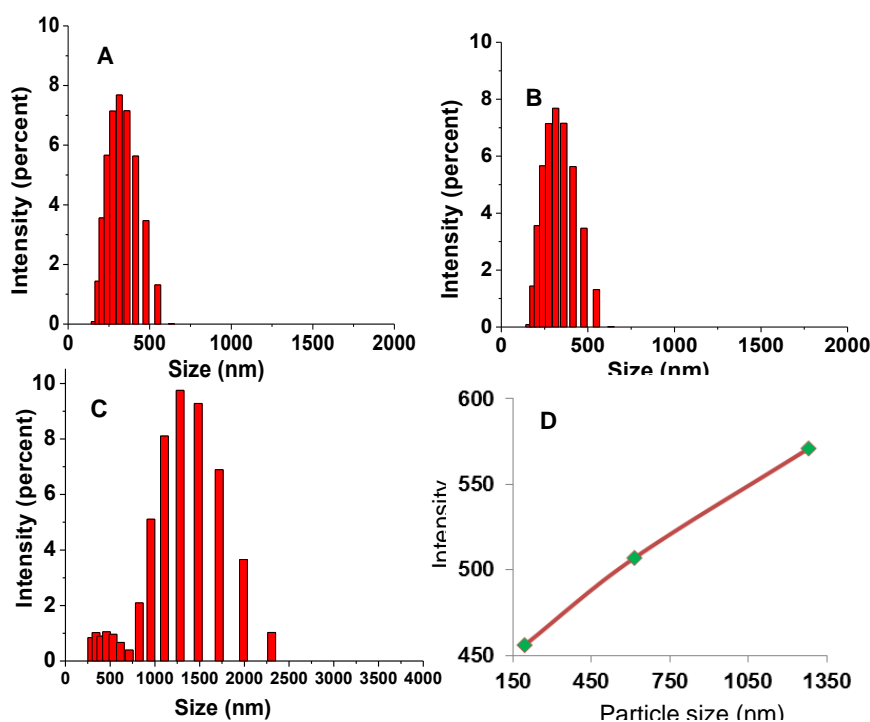


Figure 44: DLS measurements of solutions of derivative **22** (10 μ M) in different fractions of water in THF (A) 30% water/THF mixture (B) 50% water/THF mixture (C) 70% water/THF mixture (D) plot showing the variation of fluorescence emission intensity vs. particle size.

On the basis of absorption, fluorescence, DLS and time resolved studies we believe that molecules of derivatives **21** and **22** are packed in slipped fashion and restriction of intramolecular rotation along with aggregation driven growth are the main reasons for the observed emission enhancement in these derivatives. Out of derivative **21** and **22**, derivative **22** with electron donating amino groups shows higher emission enhancement which may be due the TICT state in derivative **21**. Thus, presence of electron rich substituents is beneficial for the development of triphenylene based AIEE active materials.

Table 1: Photophysical properties of derivatives **21** and **22**

Derivatives	λ abs. (nm)	Φ in THF	Φ in H ₂ O :THF mix	Emission enhancement	I/I ₀	(I-I ₀)/I ₀ ×100	τ pure THF (ns)	τ In THF H ₂ O mix. (ns)
14	307	0.29	0.44 (1:1)	1.5	1.41	41.7	6.43	7.51
20	326	0.34	0.54 (7:3)	1.6	1.44	44.47	5.72	7.37

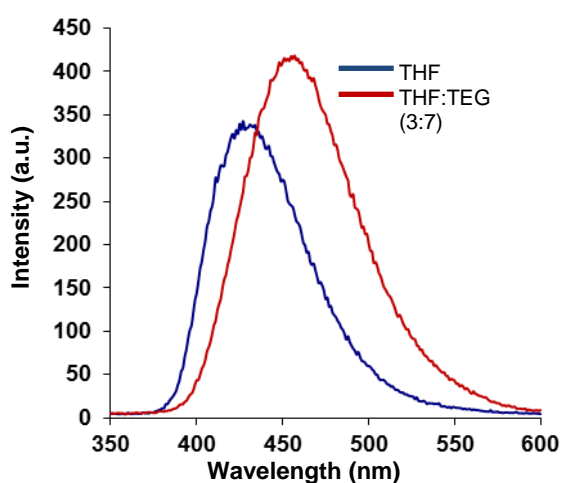


Figure 45: Fluorescence emission spectrum of derivative **22** in THF and TEG:THF (7:3) mixture.

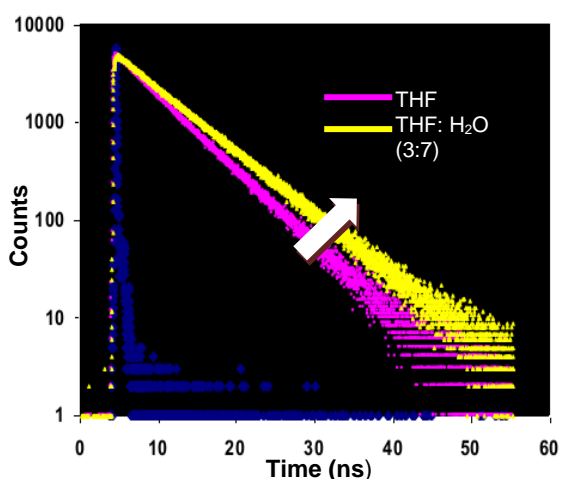


Figure 46: Time resolved fluorescence spectrum of derivative **22** (10 μ M) in THF and H₂O:THF (7:3) mixture (λ_{ex} = 377nm).

High emission intensity of aggregates of triphenylene derivatives **21** and **22** prompted us to evaluate their application as potential chemosensors for nitroaromatic explosives. Keeping this in mind, we have carried out fluorescence studies of these AIEE active triphenylene derivatives in H₂O:THF mixture with various nitro derivatives such as picric acid (PA), 2,4,6-trinitrotoluene (TNT), 2,4-dinitrotoluene (DNT), 1,4-dinitrobenzene (DNB), nitrobenzene (NB), 4-nitrotoluene (4-NT), nitromethane (NM), 2,3-dimethyl-2,3-dinitrobutane (DMNB)

and electron deficient 1,4-benzoquinone (BQ) respectively. Among the various nitroderivatives tested, addition of 20 equiv. of picric acid to the solution of derivative **21** in H₂O:THF (1:1) mixture results in 92% quenching of emission (**Figure 47**). The quenching of fluorescence of derivative **21** was studied by Stern-Volmer plot (**Figure 48**). The Stern-Volmer plot was found to be linear at lower concentration of picric acid (upto 5 equiv., **Inset figure 48**) with Stern-Volmer constant of $1.11 \times 10^5 \text{ M}^{-1}$ but at higher equivalent it bends upwards due to the superamplified quenching effect.²⁰

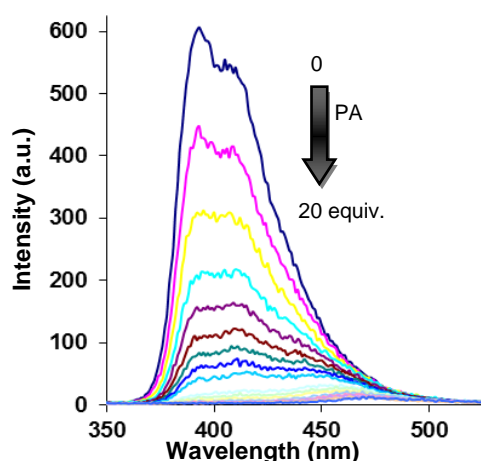


Figure 47: Fluorescence spectra of derivative **21** (10 μM) showing the variation of fluorescence intensity upon the addition of picric acid from 0-20 equiv. in H₂O:THF (1:1) mixture.

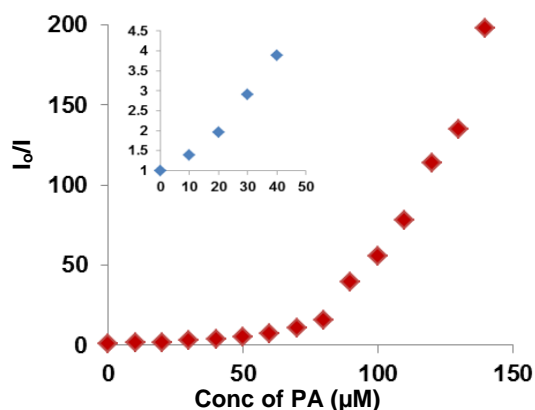


Figure 48: Stern-Volmer plot for the quenching of fluorescence of derivative **21** with PA. Inset shows the Stern-Volmer plot at lower conc. (upto 40 μM).

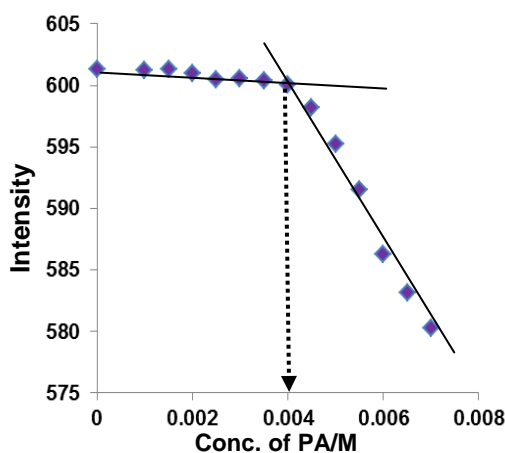


Figure 49: Plot for detection limit of derivative **15** with picric acid. (DL = $1 \times 10^{-5} \times 0.004 = 40 \times 10^{-9} = 40 \text{ nM}$).

The detection limit of derivative **21** as potential chemosensor for picric acid was found to be 40 nM (**Figure 49**). To get insight into mechanism of fluorescence quenching of derivative **14** with picric acid, we have carried out the fluorescence lifetime studies of derivative **21** at different concentrations of picric acid. The lifetime of the aggregates was found to be

invariant at different concentration of picric acid which suggests the static mechanism for the fluorescence quenching (**Figure 50**). Further, the spectral overlap of emission spectrum of derivative **21** with absorption spectrum of picric acid suggests energy transfer as probable mechanism of fluorescence quenching (**Figure 51**). Despite the presence of electron withdrawing nitrile groups, aggregates of derivative **21** exhibits sensitive response towards

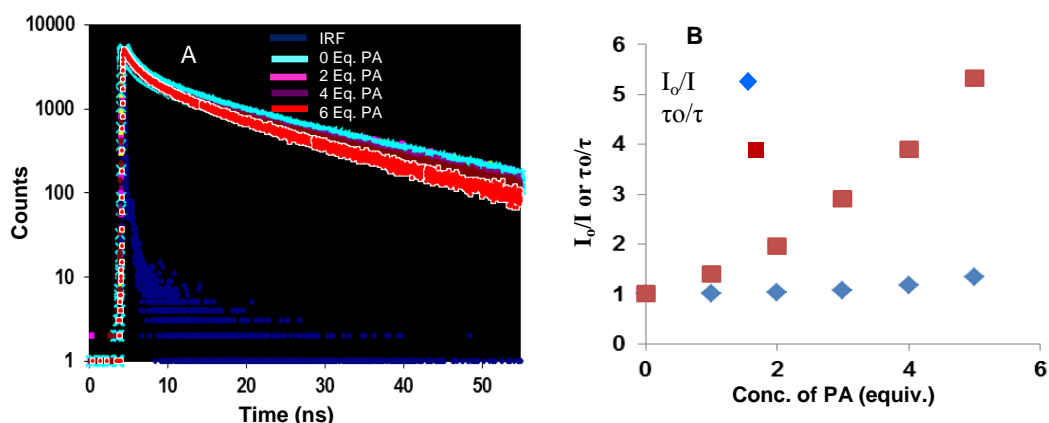


Figure 50: (A) Time resolved fluorescence spectra of derivative **21** upon the addition of different conc. of PA. (B) Stern-Volmer plot showing the change of fluorescence intensity or decay time of derivative **21** with conc. of picric acid.

picric acid. This is due to the reason that flakes like morphology of aggregates of derivative **21** provides the numerous channels for the migration of excitons resulted in higher sensitivity towards picric acid. Hence, aggregates of derivative **21** display morphology assisted sensing of picric acid.²¹

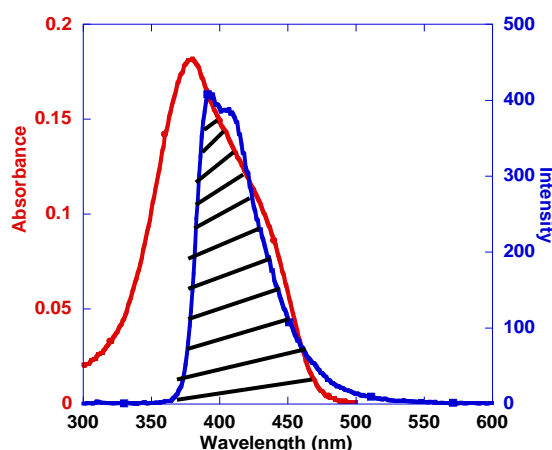


Figure 51: Spectral overlap of the absorption spectrum of picric acid (red line) with the emission spectrum of derivative **21** (blue line).

Under similar set of conditions as used for derivative **21**, we also carried out the fluorescence studies of derivative **22** with picric acid and quenching of emission was observed upon the

addition of 26 equiv. of PA (**Figure 52**) which was clearly visible to the naked eye upon illumination with UV light of 365 nm (**Inset Figure 52**). The Stern- Volmer constant was found to be $1.95 \times 10^5 \text{ M}^{-1}$ (**Figure 53**) and detection limit for PA was found to be in the range of 35 nM (**Figure 54**).

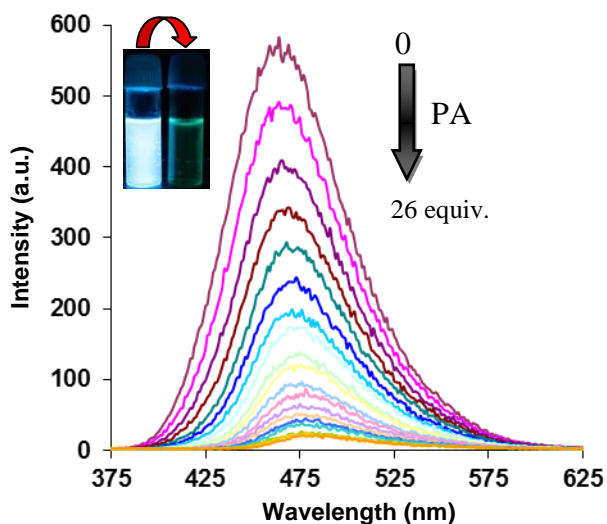


Figure 52: Fluorescence spectra of derivative **22** (10 μM) showing the variation of fluorescence intensity upon the addition of picric acid from 0-20 equiv. in $\text{H}_2\text{O}:\text{THF}$ mixture (7:3). Inset shows the image for fluorescence quenching under UV light of 365 nm.

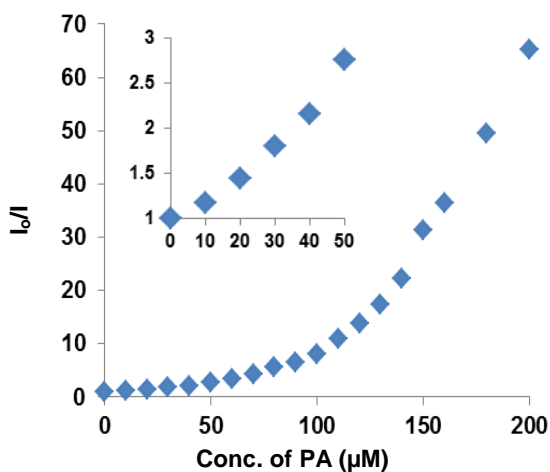


Figure 53: Stern-Volmer plot for the quenching of fluorescence of derivative **22** with PA. Inset shows the Stern-Volmer plot at lower conc. (upto 5 equiv.) of PA.

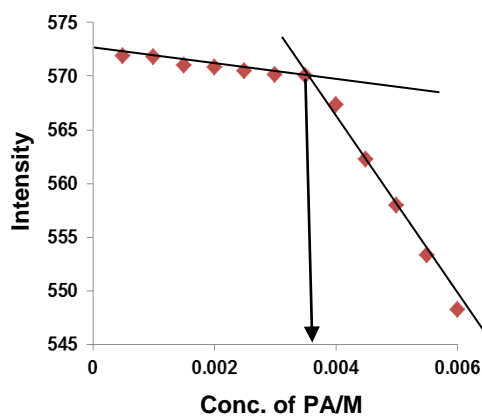
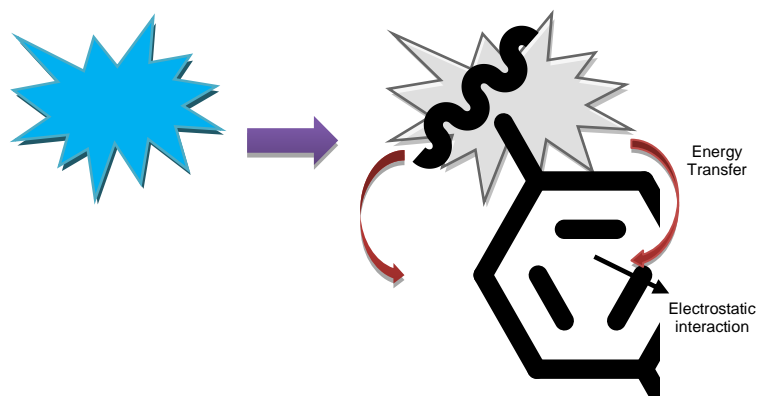


Figure 54: Plot of detection limit of derivative **22** with picric acid. $\text{DL} = 1 \times 10^{-5} \times 0.0035 = 35 \times 10^{-9} = 35 \text{ nM}$.

Picric acid is a strong acid²² and readily undergoes dissociation to give free protons which result in the protonation of basic NH_2 groups of aggregates of derivative **22**. The electrostatic interactions between aggregates of protonated form of derivative **22** with picrate ions resulted in the fluorescence quenching as shown in **scheme 8**.²³ This mechanism was further confirmed by carrying out the ^1H NMR studies of derivative **22** with picric acid in

DMSO- d_6 (Figure 55). Upon the addition of picric acid, signal corresponding to NH_2 protons disappeared completely and downfield shift is observed in the signals corresponding to the aromatic protons. Similar downfield shift in the signals was observed in the ^1H NMR studies of derivative **16** in DMSO- d_6 in the presence of trifluoroacetic acid (TFA) (Figure 55 and Table 2). These studies validate the proposed mechanism involving the electrostatic interaction between the protonated form of derivative **22** and picrate ions.



Scheme 8: Mechanism of quenching of fluorescence of derivative **22** with picric acid.

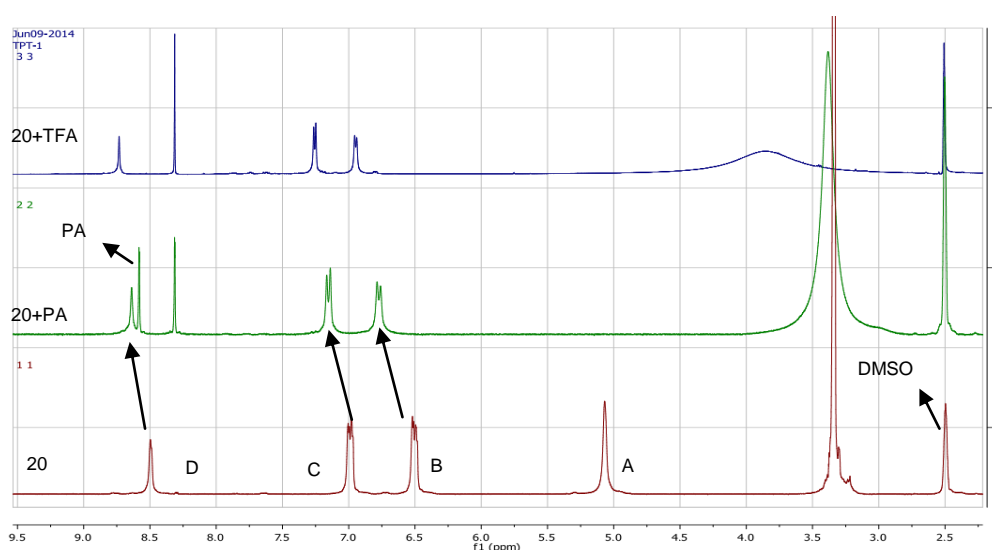


Figure 55: ^1H NMR spectrum of derivative **16** upon the addition of picric acid and TFA in DMSO- d_6

Under same conditions, we have also studied the recognition behaviour of aggregates of derivatives **21** and **22** in H_2O : THF mixture toward other nitroderivatives such as 2,4-dinitrotoluene (DNT), 1,4-dinitrobenzene (DNB), nitrobenzene (NB), 4-nitrotoluene (4-NT), nitromethane (NM) and 2,3-dimethyl-2,3-dinitrobutane (DMNB) and electron deficient 1,4-benzoquinone (BQ). The fluorescence quenching was also observed with other NACs,

however, much higher equivalents of nitroderivatives were used. The relative percentage quenching with various nitroaromatics is summarized in bar diagram by taking 20/26 equivalent of picric acid for derivatives **21** and **22** respectively (**Figure 56**). From bar diagram, it is clear that aggregates of derivatives **21** and **22** showed sensitive response

Table 2. Chemical shift in ^1H NMR of derivative **16** upon the addition of PA and TFA

S.No.	H _B	H _C	H _D
Derivative 20	6.51	6.99	8.50
Derivative 20+PA	6.77	7.15	8.63
$\Delta\delta_{\text{PA}}$	0.26	0.16	0.13
Derivative 20+TFA	6.94	7.24	8.72
$\Delta\delta_{\text{TFA}}$	0.43	0.34	0.22

towards picric acid. High sensitivity of aggregates of derivatives **21** and **22** towards picric acid may be attributed to the electron deficient nature and high polarizability of picric acid.²⁴ Moreover, the efficient energy transfer from excited state of aggregates of derivative **21** to ground state of picric acid (as evident from large spectral overlap between absorption spectrum of picric acid and emission spectrum of derivative **21**; **Figure 51**) and electrostatic interaction in case of derivative **22** account for high selectivity of aggregates of these derivatives towards picric acid.

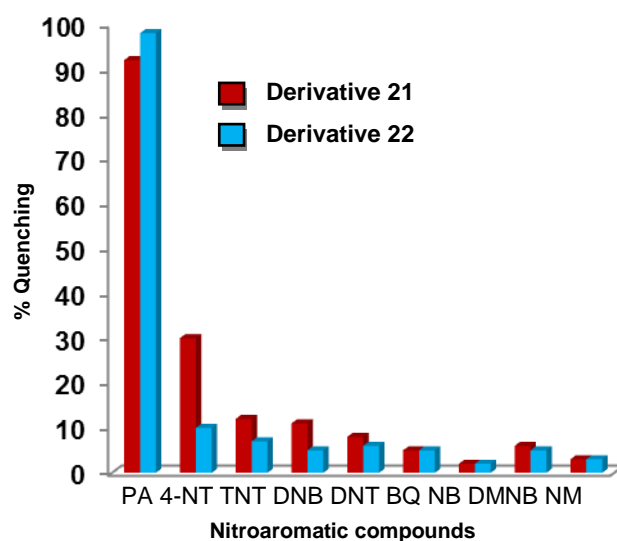


Figure 56: Bar diagram showing the %age quenching of derivatives **21** and **22** upon the addition of various nitroaromatic compounds.

Further, we have also prepared paper strips by dip coating the solution of aggregates of derivative **22** in H₂O:THF (7:3) mixture which can detect the trace amounts of picric acid in solid state. For this purpose, we prepared the aqueous solution of picric acid of varying concentrations. 10 µl of these solutions were placed over the solution coated strips of aggregates of derivative **22** covering an area of about 1 cm². The minimum amount of picric acid that can be detected by naked eye was upto 10⁻¹¹ M which corresponds to 22.9 x 10⁻¹⁵ g.cm⁻² of picric acid (**Figure 57**). The lower detection limit by solution coated test strips of derivative **22** as compared to their solution phase is due to their well-defined packing in the test strips which facilitates the faster exciton migration which amplifies the quenching process. These results show the practical applicability of derivative **22** for fast, reliable and visual on site trace detection of picric acid.

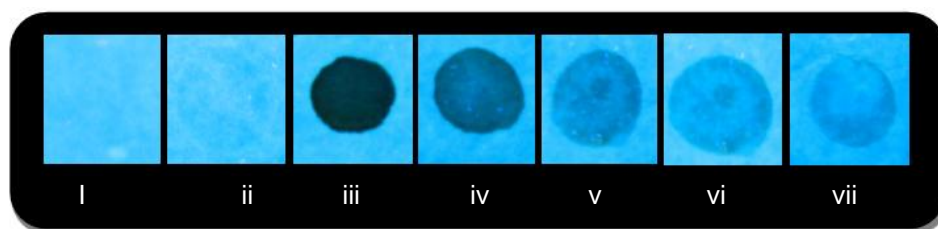


Figure 57: Photographs of solution coated paper strips of derivative **22** showing fluorescence quenching (under UV light of 365 nm); (i) blank paper strip (ii) a paper strip with a drop of water; paper strips upon the addition of 10 µl solution of PA of different concentrations (iii) 10⁻³ M (iv) 10⁻⁵ M (v) 10⁻⁷ M (vi) 10⁻⁹ M (vii) 10⁻¹¹ M.

(v) Aggregates of triphenylene derivative as reactor for the preparation of gold nanoparticles

We have also evaluated the binding behaviour of aggregates of derivative **22** with different metal ions such as Au³⁺, Pd²⁺, Cd²⁺, Ba²⁺, Pb²⁺, Hg²⁺, Ni²⁺, Zn²⁺, Cu²⁺, Co²⁺, Ag⁺, Na⁺, K⁺, Li⁺ as their perchlorate/chloride/ both perchlorate and chloride salts by UV-vis and fluorescence spectroscopy. Interestingly, fluorescent aggregates of derivative **22** exhibits sensitive response towards Au³⁺ ions and served as reactor and stabilizer for the facile preparation of spherical gold nanoparticles at room temperature without the addition of any external reducing agent.

UV-vis spectrum of aggregates of derivative **22** (10 µM) exhibits an absorption band at 325 nm in H₂O:THF (7:3) mixture (**Figure 58**). Among the various metal ions tested, derivative **22** showed selective response towards Au³⁺ ion. Upon the addition of 10 equiv. of Au³⁺ ions, the band at 325 nm decreased and ‘leveling of tail’ was observed in the visible

region of the spectrum. Further addition of Au^{3+} ions (10-15 equiv.) resulted in the appearance of a new band at 545 nm (**Inset Figure 58**) which corresponds to the surface plasmon resonance (SPR) band of gold nanoparticles.²⁵ Within 15 minutes, the colour of the resulting solution changed from pale yellow to violet. The color change and appearance of new band in the range of 500-600 nm indicates the formation of gold nanoparticles. However, with other metal ions tested, insignificant changes were observed in their UV-vis spectra.

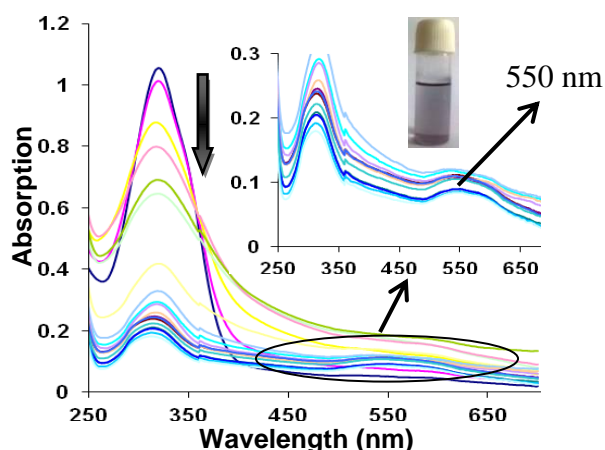


Figure 58: UV-vis spectra of derivative **22** (10 μM) in H_2O :THF (7:3) upon the addition of Au^{3+} ions (15 equiv.).

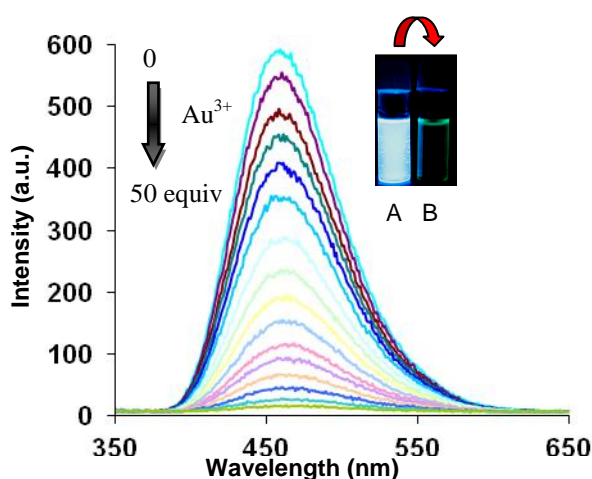


Figure 59: Fluorescence spectra of derivative **22** (5 μM) upon the addition of Au^{3+} (0 to 50 equiv.) in H_2O :THF (7:3) mixture. Inset shows the fluorescence images of derivative **22** (A) before (B) after the addition of Au^{3+} ions.

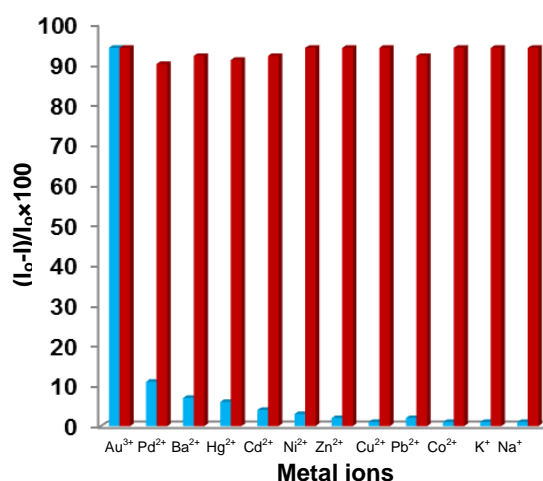


Figure 60: Bar diagram showing the selectivity (blue bars) and competitive selectivity (red bars) of derivative **22** towards Au^{3+} ions among various cations in H_2O :THF (7:3) mixture.

The fluorescence spectrum of aggregates of derivative **22** ($\Phi = 0.54$) showed quenching of fluorescence upon the addition of 50 equiv. of Au^{3+} ions (**Figure 59**). The

observed fluorescence quenching may be attributed to the binding of Au³⁺ ions to the aggregates of derivative **22**. Under the same conditions as used for Au³⁺ ions, we also carried out the fluorescence studies of aggregates of derivative **22** with other metal ions (Pd²⁺, Cd²⁺, Ba²⁺, Pb²⁺, Hg²⁺, Ni²⁺, Zn²⁺, Cu²⁺, Co²⁺, Ag⁺, Na⁺, K⁺, Li⁺ as their perchlorate/chloride/ or both perchlorate and chloride salts), however, no significant change in the fluorescence intensity was observed (**Figure 60**). Hence, aggregates of derivatives **22** acts as selective chemosensor for Au³⁺ ions. The calculated detection limit of derivative **22** for Au³⁺ ions was found to be 55 nM (**Figure 61**). To test the practical application of aggregates of

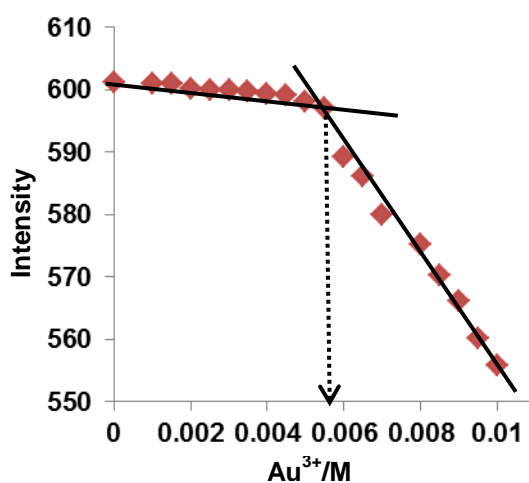


Figure 61: Plot for detection limit of derivative **22** for Au³⁺ ions. DL = $1 \times 10^{-5} \times 0.0055 = 55 \times 10^{-9} = 55$ nM.

derivative **22** as selective chemosensor for Au³⁺ ions, competitive studies were carried out in the presence of 50 equivalents of Au³⁺ ions (**Figure 60**) mixed with Pd²⁺, Cd²⁺, Ba²⁺, Pb²⁺, Hg²⁺, Ni²⁺, Zn²⁺, Cu²⁺, Co²⁺, Ag⁺, Na⁺, K⁺, Li⁺ at 200 equivalents but no significant variation in the fluorescence emission was observed by comparison with and without the other metal ions.

The UV-vis and fluorescence studies suggest the interaction of Au³⁺ ions with amino groups of the aggregates of derivative **22** and their subsequent reduction to Au(0) ions. The reduction process involves the compartmentalization mechanism²⁶ as in the case of micellar aggregates.²⁷ Here, the aggregates with network of interconnected channels may be regarded as reactors where the metal complexes are reduced. Hence, upon the addition of Au³⁺ ions to the solution of aggregates of derivative **22**, the Au³⁺ ions interact with amino groups and get reduced.²⁸ The formation of gold nanoparticles was further confirmed by transmission

electron microscope (TEM), powder X-ray diffraction (XRD) and energy-dispersive X-ray spectroscopy (EDX) analysis. TEM image of derivative **22** in the presence of gold ions showed nearly spherical gold nanoparticles having size in the range of 10 to 110 nm (**Figure 62a-b**). The powder XRD analysis of the nanoparticles showed the characteristic XRD pattern which corresponds to the 111, 200, 220 and 311 planes of a face centered cubic (fcc) lattice of gold²⁹ with peaks at 2θ value of 37.75, 43.99, 64.21 and 77.24 (**Figure 63**). Further, the EDX spectrum of derivative **22** in the presence of gold ions confirmed the presence of gold nanoparticles (**Figure 64**).

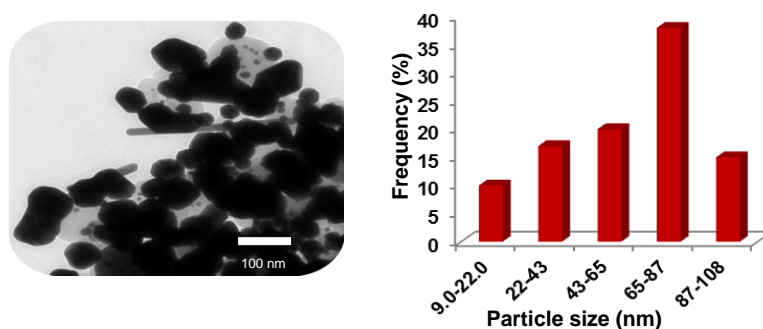


Figure 62: (a) TEM image of gold nanoparticles of derivative **22**; (b) Size distribution of gold nanoparticles.

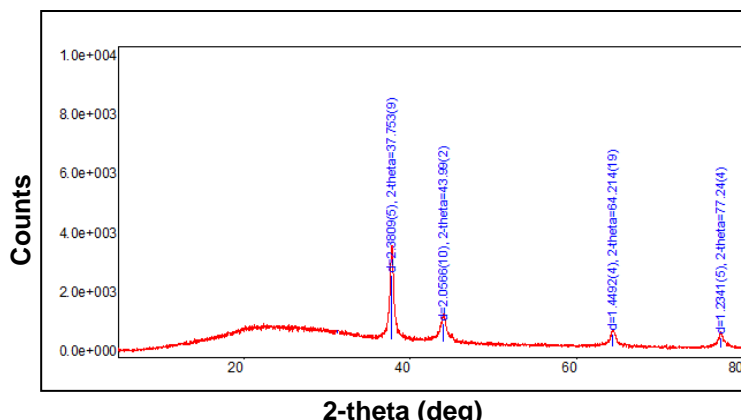


Figure 63: Powder X-ray diffraction (XRD) pattern of gold nanoparticles of derivative **22** after drying the sample in ambient conditions.

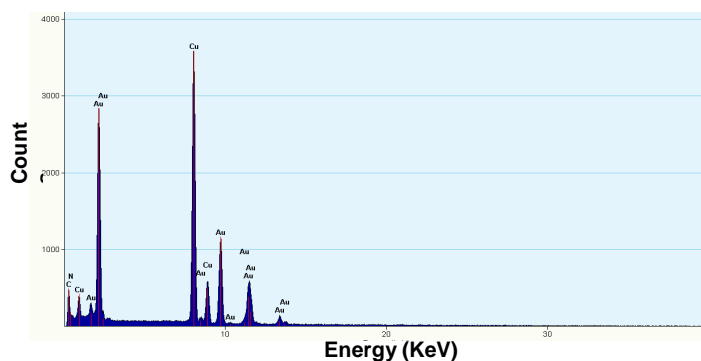


Figure 64: EDX spectra of gold nanoparticles of derivative **22** on copper grid.

Scheme 9: Reduction of 4-Nitrophenol to 4-aminophenol in the presence of NaBH₄ using amine stabilized gold nanoparticles as catalyst.

We also investigated the catalytic activity of *in situ* generated gold nanoparticles in the reduction reaction of 4-nitrophenol to 4-aminophenol (**Scheme 9**) in aqueous medium in the presence of NaBH₄ by UV-vis spectroscopy.³⁰ 4-nitrophenol showed an absorption band at 317 nm in aqueous medium (**Figure 65 A**). Upon the addition of NaBH₄, the band at 317 nm shifted to 400 nm and colour of the solution changed from pale to yellow due to the formation of phenolate ions. Further, upon the addition of catalytic amount of *in situ* generated gold nanoparticle solution (10 μ l), the intensity of band at 400 nm decreased gradually and a new band was appeared at 300 nm. The appearance of new band suggested the formation of 4-aminophenol. The whole reaction was completed in 12 minutes and rate constant was found to be $0.759 \times 10^{-2} \text{ sec}^{-1}$ (**Figure 65 B-C**). The blank experiment was also carried out for the reduction of 4-nitrophenol with NaBH₄ in the absence of *insitu* generated gold nanoparticles and very slow decrease in the absorption band at 400 nm was observed even after 24 hours (**Figure 66**). This study shows the importance of gold nanoparticles in accelerating the reduction process in the presence of NaBH₄.

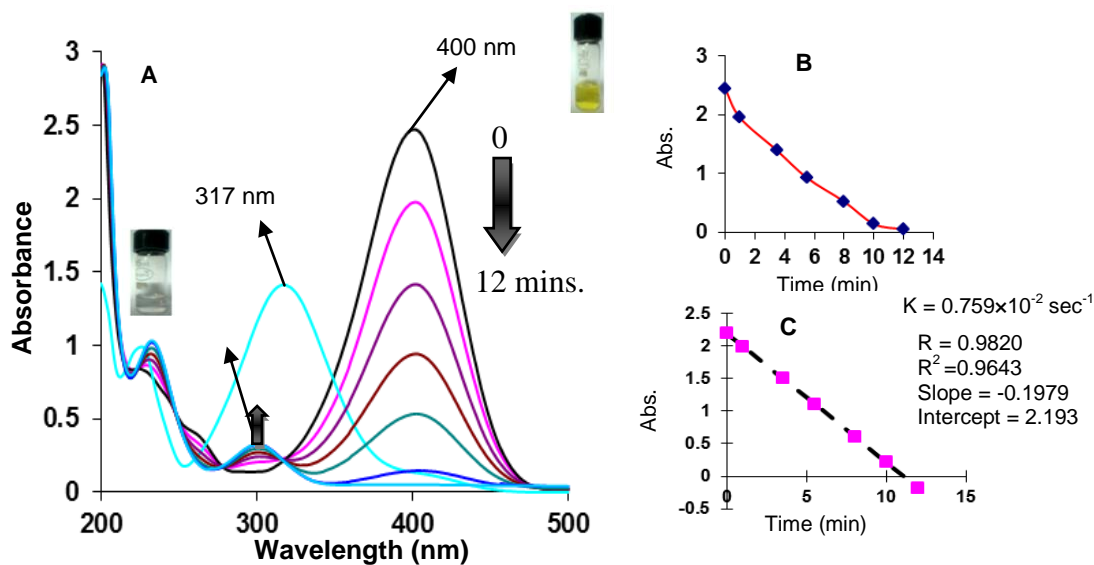


Figure 65: (A) Time dependent UV-vis absorption for the reduction of 4-Nitrophenol by NaBH₄ upon the addition of AuNPs of derivative **22** in aqueous media at room temperature (B) Plot of absorbance at 400 nm as the function of time (C) Regression plot for plot B.

To conclude, we designed and synthesized triphenylene derivatives **21** and **22** which form fluorescent aggregates in aqueous media due to the synergistic effect of slipped packing of molecules, restriction of rotation and aggregation driven growth of aggregates. Further, the aggregates of these discotic molecules act as potent chemosensor for picric acid and can detect trace amount of picric acid upto nanomolar range in aqueous medium and solution coated coated test strips of derivative **22** can detect upto $22.9 \times 10^{-15} \text{ g.cm}^{-2}$ of picric acid

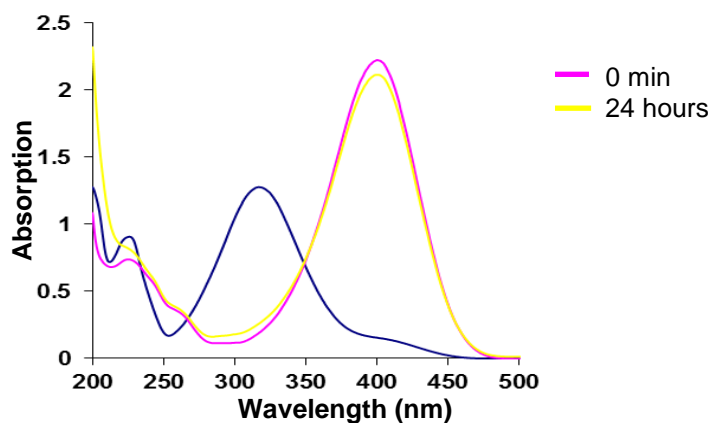


Figure 66: Time dependent UV-vis absorption spectrum for the reduction of 4-Nitrophenol by NaBH_4 in the absence of gold nanoparticles.

which provides a cheap, portable and easily accessible method for the onsite detection of picric acid explosive. Furthermore, fluorescent aggregates of triphenylene derivative **22** served as reactors and stabilizers for the facile preparation of gold nanoparticles at room temperature without the addition of any external stabilizing or reducing agent. Additionally, the *in situ* generated gold nanoparticles smoothly catalyzed the reduction of 4-nitrophenol to 4-aminophenol with NaBH_4 in aqueous medium.

(vi) Aggregates of Gallic Acid Substituted Triphenylene Derivative for the Sensitive Detection of Trinitrotoluene in Aqueous Medium and in Vapour Phase

Alkylated gallic acid **26** was synthesized by reported method.³¹ Gallic acid, **23** was protected by esterification to yield derivative **24** which upon alkylation with *n*-bromohexane followed by deprotection with aq. KOH gave alkylated gallic acid **26**. Refluxing of alkylated gallic acid with thionyl chloride lead to the formation of alkylated gallic acid chloride **27** (**Scheme 10**). Finally, the condensation of gallic acid chloride **27** with triphenylene hexamine **22** in dry

Scheme 10



THF under nitrogen atmosphere at 0°C furnished derivative **28** in 60% yield (**Scheme 11**). The structure of derivative **28** was confirmed from its spectroscopic and analytical data. The ¹H NMR spectrum of compound **28** in CDCl₃ showed five signals at δ 0.90 (54H), 1.34 (36H), 1.49-1.56 (72H), 1.74-1.82 (36H), 4.02 (36H) corresponding to the aliphatic protons, four signals at 7.07 (12H, ArH), 7.365 (12H, ArH), 7.585 (12H, ArH), 8.59 (6H, ArH) and a signal at 7.78 (6H, NH) corresponding to the aromatic and amide protons respectively. The structure of derivative **28** was further confirmed from MALDI-TOF mass spectrum which showed a peak at 3222.6223 (M+Na⁺). Further the FT-IR spectrum of derivative **28** showed a peak at 1648.17 cm⁻¹ corresponding to carbonyl group stretching and a broad peak at 3431.64 correspond to NH amide stretching which confirms the presence of amide bond in derivative **28**. These spectroscopic data corroborate the structure **28** for this compound.

In the UV-vis spectrum derivative **28** shows an absorption band at 319 nm when dissolved in THF (**Figure 67A**). Upon increasing the water fraction from 0 to 70 % volume in THF solution of derivative **28**, broadening of absorption signal along with a bathochromic shift of 11 nm is observed. In addition, the ‘leveling off tail’ was observed in the visible region of spectrum (**Inset, Figure 67A**). This leveling of tail indicates the formation of aggregates of derivative **28**. The fluorescence spectrum of derivative **28** exhibits a broad emission band at

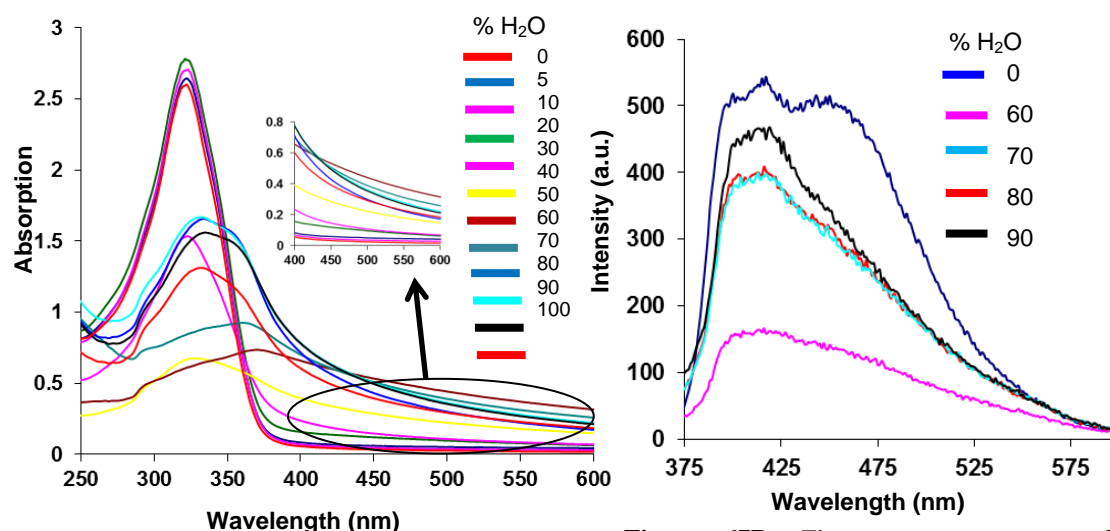


Figure 67A: UV-vis spectrum of derivative **28** (10 μ M) in different fractions of water in THF.

Figure 67B: Fluorescence spectrum of derivative **28** in different fractions of water in THF.

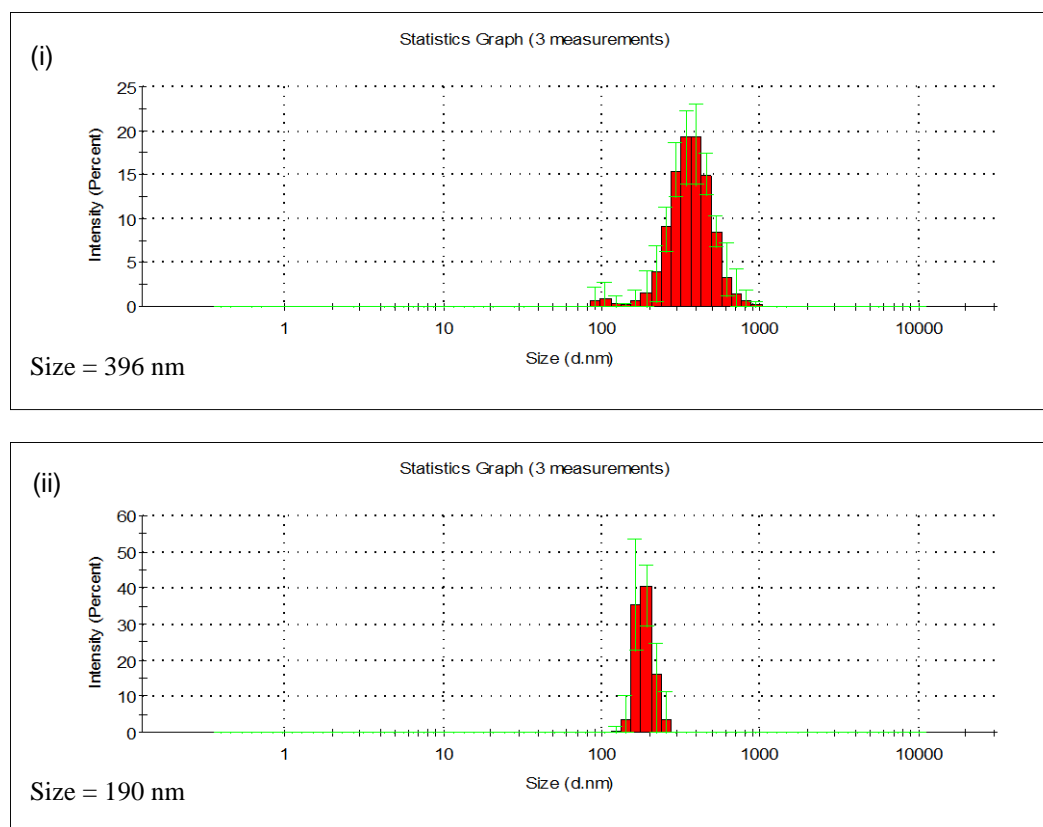


Figure 68A: Dynamic light scattering (DLS) results showing the variation of particle size diameter of derivative **28** in (i) H₂O:THF (3:7), (ii) H₂O:THF (1:1) mixture respectively.

417 nm when excited at 319 nm (**Figure 67B**). Increasing the water fraction from 0 to 60 % resulted in the decrease in emission intensity. Further addition of water fraction upto 90% resulted in the increase in increase in emission intensity. The dynamic light scattering (DLS) studies clearly showed average size of aggregates around 396 nm, 190 nm, 141 nm and 91 nm in 30%, 50%, 70%, and 90% H₂O/THF solvent mixture respectively (**Figure 68A-B**). From these studies we assume that particles tend to shrink in size with the increase in water content in solvent mixture. A more coplanar conformer imposed by the congested environment in the shrunk particles may be responsible for emission enhancement.³²

The scanning electron microscopic (SEM) image of derivative **28** shows the presence of porous aggregates (**Figure 69A-B**). The polarized optical microscope (POM) image of well dried aggregates of derivative **28** showed star shaped texture upon cooling which suggests the formation of ordered aggregates in H₂O/THF mixture (**Figure 69C**). Further, effect of

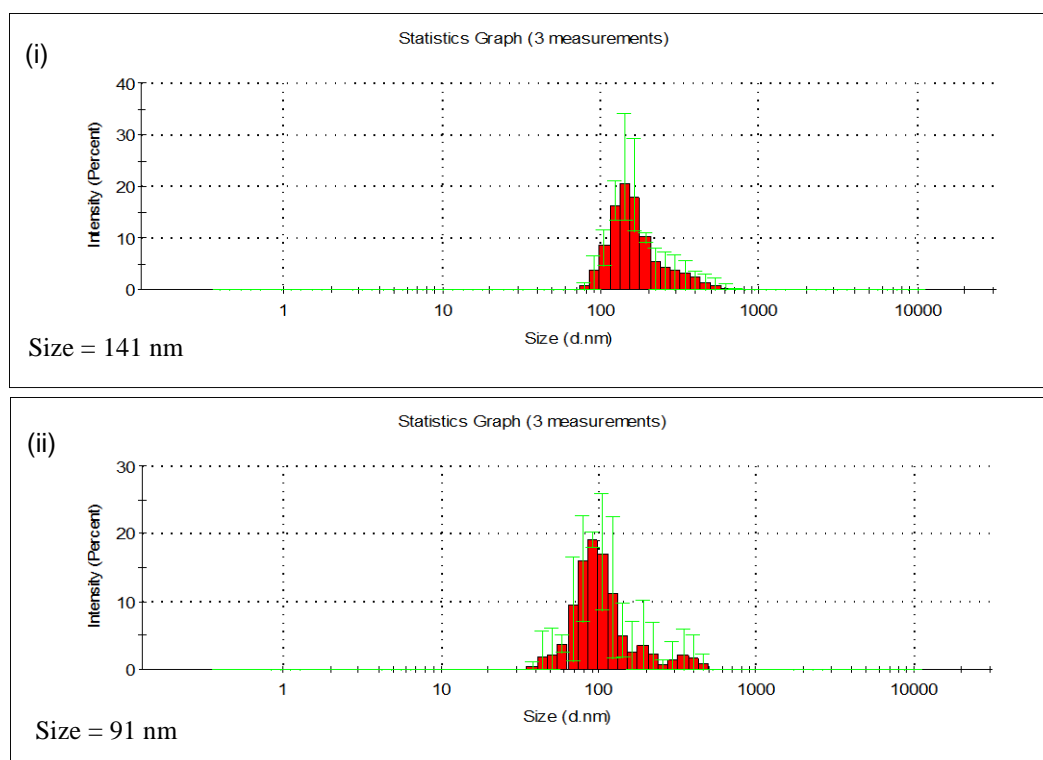


Figure 68B: Dynamic light scattering (DLS) results showing the variation of particle size diameter of derivative **28** in (i) H₂O :THF (7:3) and (ii) H₂O :THF (9:1) mixture respectively.

increasing concentration was studied by concentration dependent ¹H NMR studies in CDCl₃. Upon increasing the concentration, upfield shifting and the broadening of signals corresponding to aromatic protons was observed (**Figure 70**). Such an upfield shift may be

attributed to the intermolecular shielding from the neighboring aromatic molecules in the concentrated solution indicating the π - π stacking of derivative **28** upon increasing the concentration.³³

On the basis of all these studies, we propose that upon self-assembly, the molecules of derivative **28** form π - π stacked units which are interconnected through hydrogen bonds in slipped fashion to form a closely packed fluorescent supramolecular polymer.

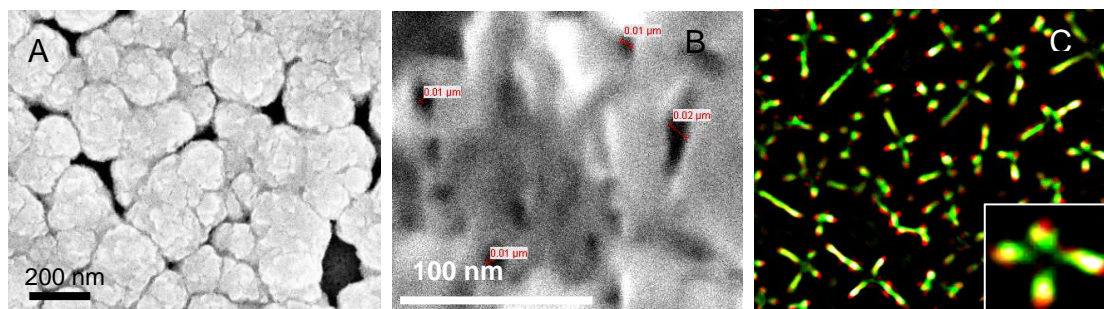


Figure 69 (A-B) Scanning Electron microscope (SEM) images derivative **28** in H₂O:THF (9:1) (C) POM image of aggregates of derivative **28** at room temperature after cooling from 350 °C. Inset show magnified image.

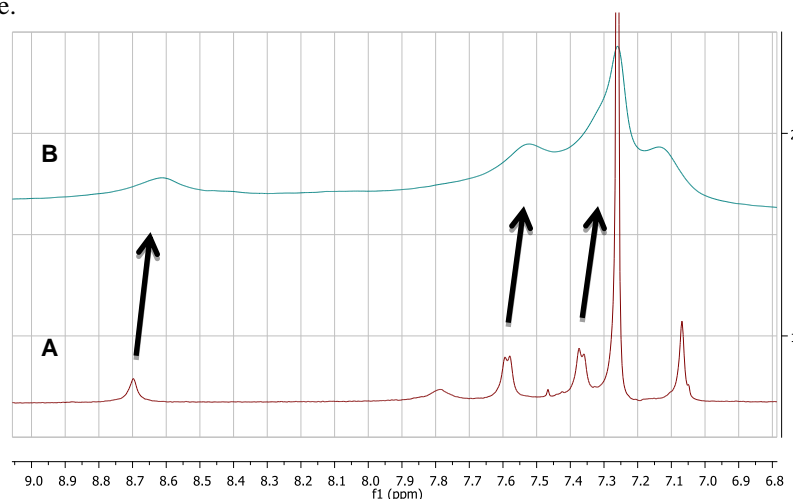


Figure 70: Change in partial ¹H NMR spectrum of derivative **28** upon increasing the concentration from (A) 2mg/0.6ml to (B) 10 mg/0.6 ml in CDCl₃.

Further, the high emission intensity of derivative **28** in H₂O:THF (9:1) mixture ($\Phi=0.4$)³⁴ prompted us to explore potential application of these aggregates as chemosensor for the detection of nitroaromatic compounds such as 2,4,6-trinitrotoluene (TNT), 2,4,6-trinitrophenol (TNP), 2,4-dinitrotoluene (DNT), 1,4-di-nitrobenzene (DNB), 4-nitrotoluene (NT), 2,4-dinitrophenol (DNP), other nitroderivatives such as nitromethane (NM), 2,3-dimethyl-2,3-dinitrobutane (DMNB) and electron deficient 1,4-benzoquinone (BQ). The emission of derivative **28** in H₂O:THF (9:1) mixture was completely quenched upon the addition of 0.15 equiv. of TNT (**Figure 71A**). This quenching of fluorescence was clearly

visible to naked eye when observed under the UV light of 365 nm (**Inset, Figure 71A**). The quenching of fluorescence with TNT was studied by Stern-Volmer relationship (**Figure 71B**). The Stern-Volmer plot of derivative **28** was found to be hyperbolic curved which was straight line at lower concentration (upto 0.75 μM , **Inset, Figure 71B**) with Stern-Volmer constant of $13.33 \times 10^5 \text{ M}^{-1}$ but at higher concentration it bends upwards due to superamplified quenching effect.³⁵

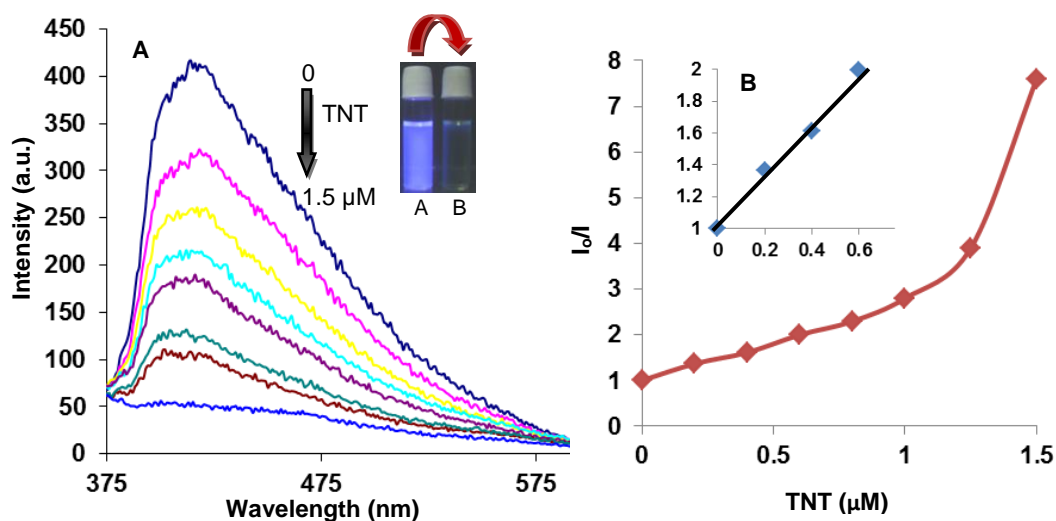


Figure 71(A): Fluorescence emission spectrum of derivative **28** ($10 \mu\text{M}$) upon the addition of 2,4,6-trinitrotoluene (TNT) from 1 to $4 \mu\text{M}$ in $\text{H}_2\text{O}:\text{THF}$ (1:9) mixture. Inset shows the fluorescence of derivative **28** (A) before and (B) after the addition of TNT (**B**) Stern-Volmer plot for the quenching of derivative **28** with TNT. Inset shows the Stern-Volmer plot at low concentration.

The detection limit of aggregates of derivative **28** for TNT was found to be 56.75 ppq (**Figure 72**) which is much below that the maximum limit for TNT in drinking water as set by US EPA. The calculated limit of detection (LOD) is also very low as compared to other reported chemosensors for TNT. We also carried out the fluorescence studies of derivative **28** with TNT in THF and only 35% quenching was observed upon the addition of $1.5 \mu\text{M}$ of

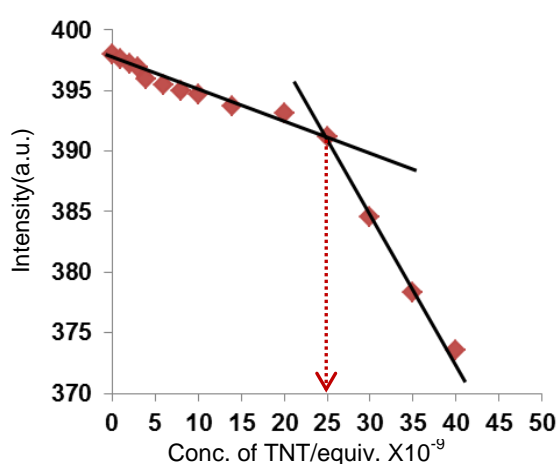


Figure 72: Plot for the detection limit of derivative **28** ($10 \mu\text{M}$) with TNT (detection limit = $1 \times 10^{-5} \times 25 \times 10^{-9} = 25 \times 10^{-14} = 56.75 \text{ ppq}$).

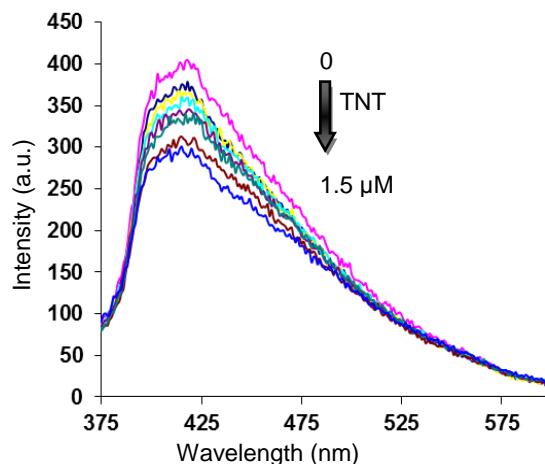


Figure 73: Fluorescence emission spectrum of derivative **28** ($10 \mu\text{M}$) upon the addition of $1.5 \mu\text{M}$ of TNT in pure THF.

TNT (**Figure 73**). We believe that presence of porous aggregates in H₂O: THF (9:1) provides eliminate the possibility of energy transfer mechanism for the observed numerous channels for diffusion of TNT molecules which is responsible for the lower detection limit of derivative **28** towards TNT in mixed aqueous media.³⁶ Further, there is no spectral overlap between absorption spectrum of TNT and emission spectrum of derivative **28** (**Figure 74**) which eliminate the possibility of energy transfer mechanism for the observed fluorescence quenching. Further, the absorption spectrum of derivative **28** showed a tail upon the addition of TNT (**Figure 75**). This appearance of tail may be attributed to the interaction of aggregates of derivative **21** with TNT which facilitates the charge transfer mechanism. The charge transfer mechanism was supported by cyclic voltammetric studies (**Figure 76**). The HOMO energy level of derivative **28** was found to be -5.84 eV by taking -4.8 eV as HOMO of ferrocene/ferrocenium redox system. From band gap (calculated from absorption spectrum), the LUMO energy level of derivative **28** was found to be -2.54 eV. The higher value of LUMO of derivative **28** facilitates the jump of electron to lower lying LUMO of TNT (LUMO = -3.78 eV).

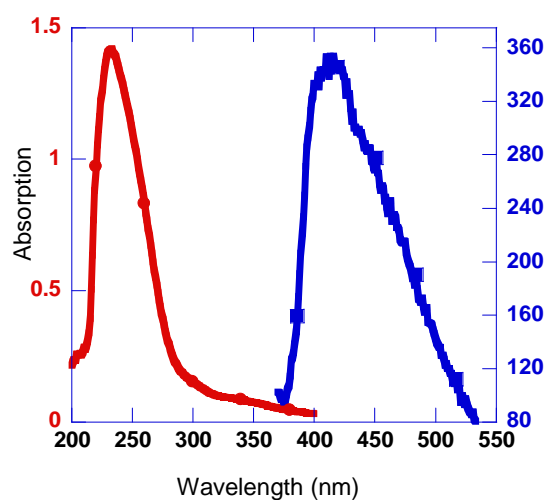


Figure 74: Spectral overlap of absorption spectrum of 2,4,6-Trinitrotoluene (red line) and emission spectrum (blue line) of derivative **28**.

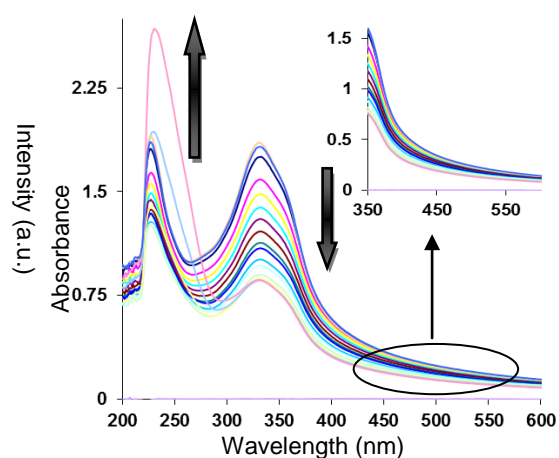


Figure 75: UV-Vis spectrum of derivative **28** (10 μ M) upon the addition of 15 μ M of TNT. Inset shows the trail in the absorption spectrum.

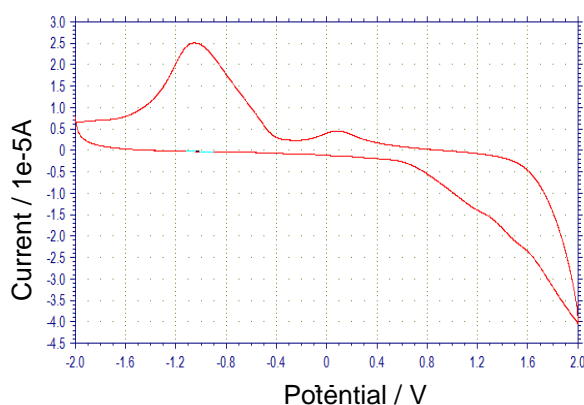


Figure 76: Cyclic Voltammogram of derivative **28** (1×10^{-3} M) in dichloromethane.

Further, we also carried out time resolved fluorescence studies of aggregates of derivative **28** in the absence and presence of different concentrations of TNT in H₂O:THF (9:1) mixture (**Figure 77A**). Derivative **28** showed lifetime of 4×10^{-12} s in the absence of TNT. However, the life time decreased (0.658×10^{-12} s) upon addition of TNT (0 to 1.5 μ M) which shows that quenching is dynamic in nature. Further, plot of change of decay time vs concentration of TNT is hyperbolic curve (**Figure 77B**) which supports the dynamic nature of fluorescence quenching due to the charge transfer from derivative **28** to electron deficient TNT.³⁷

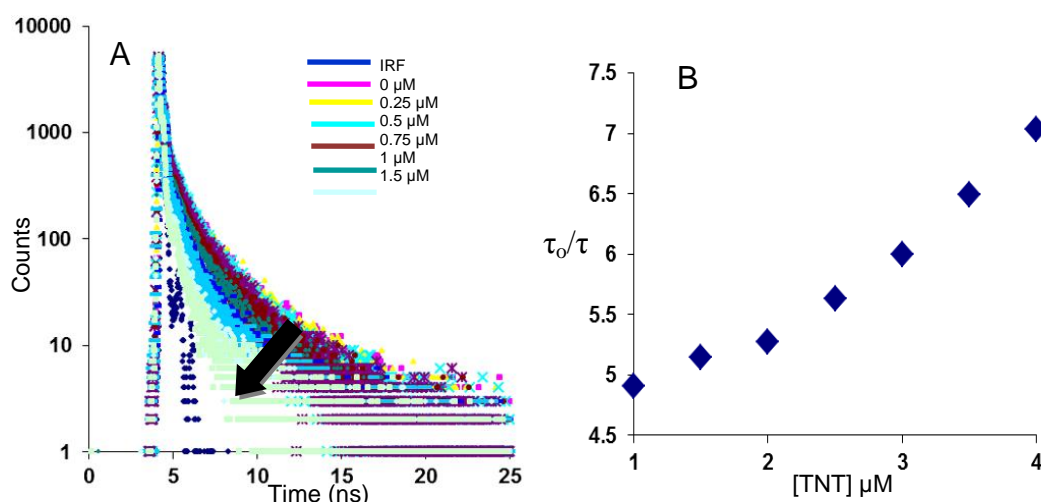


Figure 77: (A) Time resolved fluorescence spectrum of derivative **28** upon increasing the concentration of TNT from 0 μ M to 1.5 μ M. (B) Stern-Volmer plot for decay time of derivative **28** vs. concentration of TNT

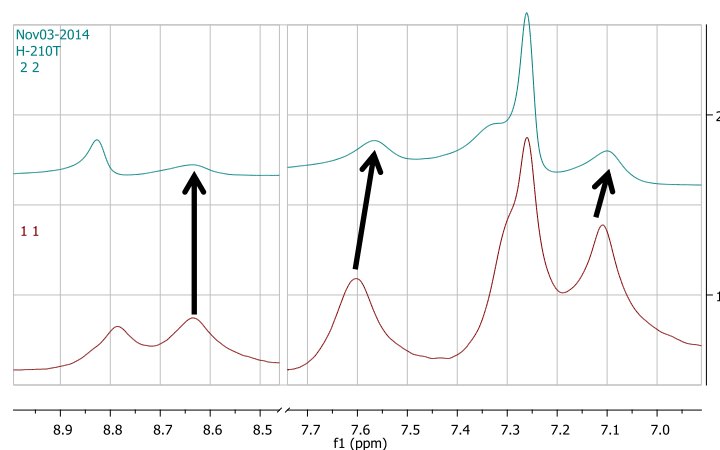


Figure 78: Partial ¹H NMR of derivative **28** upon the addition of TNT in CDCl₃.

To get insight into the mechanism of TNT sensing, we also carried out the ¹H NMR studies of derivative **28** in the presence of TNT (**Figure 78**). Upon the addition of TNT, broadening of the signal corresponding to triphenylene protons and slight upfield shift of other aromatic protons is observed. These changes in the NMR spectra confirm charge transfer mechanism.

Further, we have also carried out the DLS studies of derivative **28** in the presence of TNT. Addition of TNT (from 0 to 1.5 μM) resulted in the increase in size of aggregates from 90 to 190 nm (**Figure 79**) which can be attributed to closed interaction of TNT with aggregates of derivative **28** (**Figure 80**) which results in the fluorescence quenching in aqueous medium.

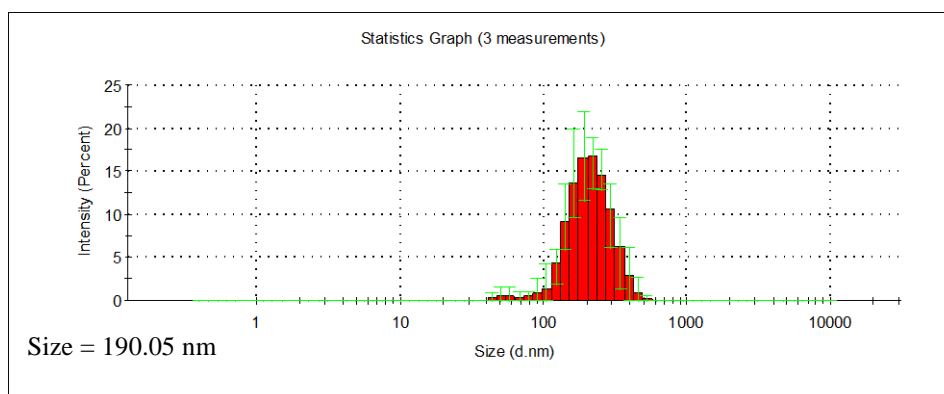


Figure 79: Dynamic light scattering (DLS) measurement of derivative **28** upon the addition of TNT (1.5 μM) in H_2O : THF (9:1) mixture.

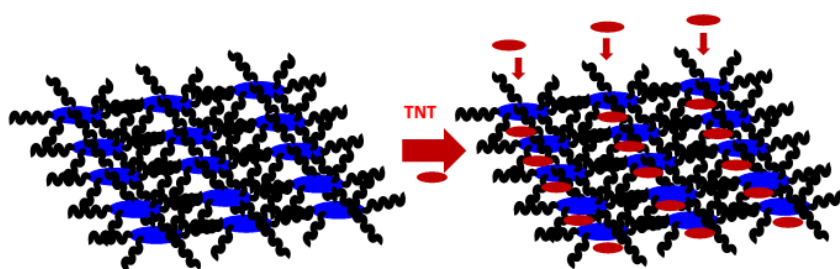


Figure 80: Schematic representation of sensing of TNT by aggregates of derivative **28**.

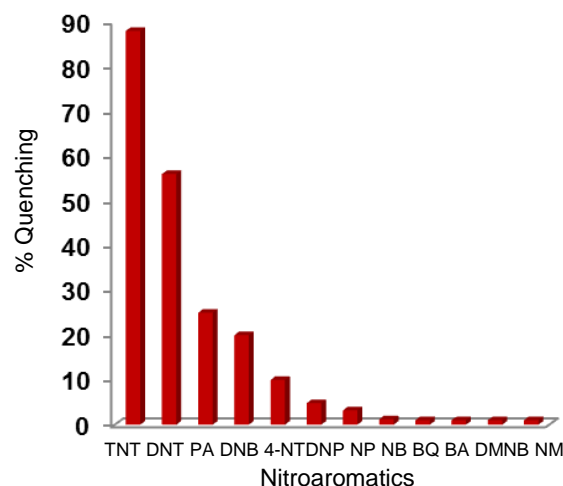


Figure 81: Bar diagram showing the percentage quenching of fluorescence of derivative **28** with various nitroaromatic compounds in H_2O :THF (9:1) mixture.

Under the same conditions as used for TNT, we have also tested fluorescence response of derivative **28** with other nitroaromatic compounds. The quenching was also observed with DNT (56%), PA (25%), DNB (20%) 4-NT (10%), DNP (5%), NP (3%) upon the addition of

1.5 μM of these NACs (**Figure 81**). However, in case of nitro derivatives (NB, DMNB and NM) and electron deficient compounds (BQ and BA) negligible quenching was observed. Thus, aggregates of derivative **28** exhibit more sensitive response towards TNT as compared to other nitroaromatics.

For the vapour phase detection of TNT, we exposed the aggregates of derivative **28** in $\text{H}_2\text{O}:\text{THF}$ (9:1) to the vapours of TNT by placing the vial containing solution in the big vial containing solid TNT at base and then fluorescence spectrum of this solution was recorded after particular time interval. Aggregates of derivative **28** showed 10% quenching of fluorescence within the 2 minutes of exposure to TNT vapours (**Figure 82A-B**) however, further exposure to TNT vapors upto 6 minutes resulted in 16 % quenching of fluorescence (**Figure 82A-B**). Thus, aggregates of derivative **28** can detect TNT in aqueous medium and in vapor phase.

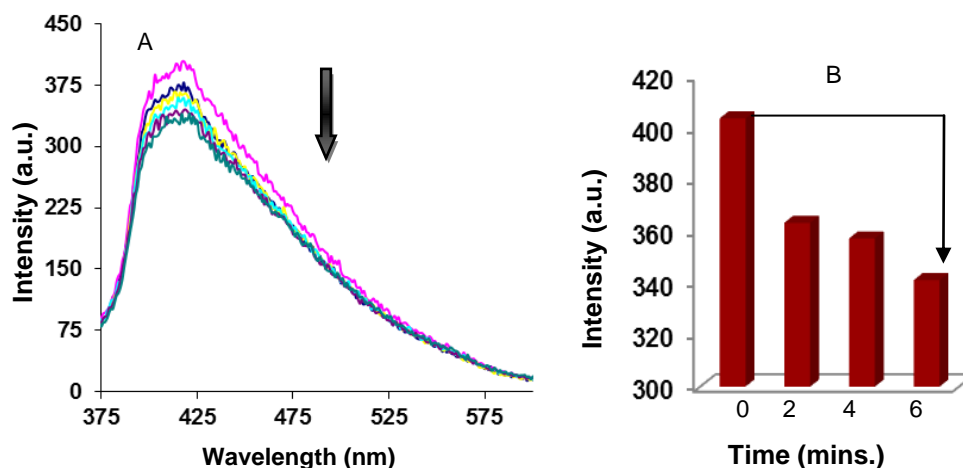


Figure 82: (A) Fluorescence emission spectrum of derivative **28** (10 μM) in $\text{H}_2\text{O}:\text{THF}$ (9:1) upon exposing it to vapors of 2,4,6-trinitrotoluene (B) Bar diagram showing the change in emission intensity of derivative **28** with time upon exposure to the vapours of TNT.

To detect trace amounts of TNT, we have prepared the solution coated test strips of derivative **28** by dipping it in the solution of derivative **28** in $\text{H}_2\text{O}:\text{THF}$ (9:1) followed by drying it under vacuum. The test strip when dipped in 10^{-5} M solution of TNT showed complete quenching of fluorescence (**Figure 83; I**). To detect the trace amounts of TNT, 10 μl of TNT solutions of different concentrations were poured over the solution coated test strips covering the $\sim 0.1 \text{ cm}^2$, the dark spots of different intensities were formed (**Figure 83; II**) which showed the regulation of intensities of spots with the concentration of analyte. The minimum concentration of TNT which can be detected was upto 10^{-12} M which corresponds to 22.7 agcm^{-2} . Further, the thin film of derivative **28** formed by drop casting method on glass

slide also showed instant quenching upon addition of a drop of TNT solution on it (**Figure 83; III**). The vapor phase sensing of TNT was performed in solid state by exposing the thin film of derivative **28** on glass slide to the vapours of TNT by placing it over the vial containing solid TNT for 5 minutes. The film showed quenching of fluorescence under the UV light of 365 nm (**Figure 83; IV**)

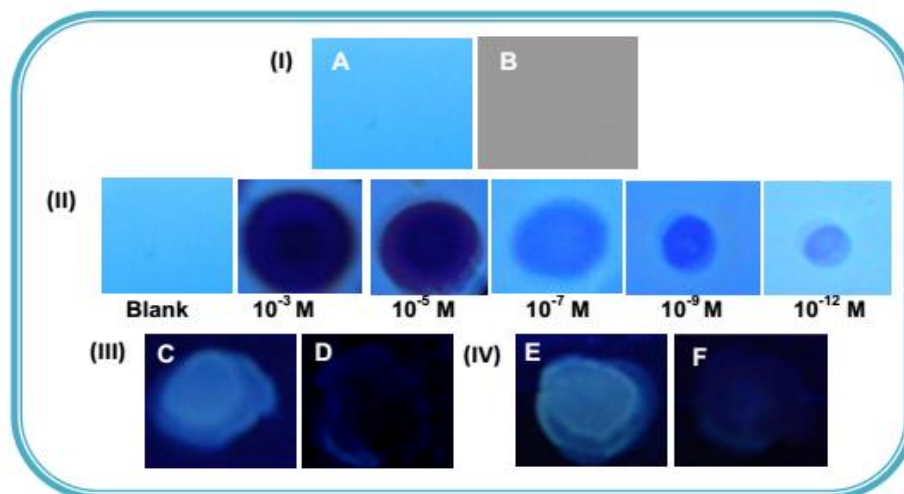


Figure 83: Fluorescent test strips of derivative **28** for the detection of TNT. **I**) A) Test strip B) Test strip dipped in 10^{-5} M solution of TNT **II**) Test strips with different concentrations of TNT **III**) c) Thin film of derivative **28** on glass slide and D) after adding one drop of TNT solution (10^{-5} M in THF) **IV**) Vapor phase sensing of TNT with thin film of derivative **28**.

In conclusion, we have designed and synthesized gallic acid appended extended triphenylene derivative **28** having amide linkages. The derivative **28** formed porous aggregates in $\text{H}_2\text{O}:\text{THF}$ (9:1) mixture. Among the various nitroaromatic explosives tested, these aggregates serve as potent chemosensor for nanomolar detection of 2,4,6-trinitrotoluene (TNT) in aqueous medium and in vapor phase. The practical application of derivative **28** as TNT chemosensor was realized by making the solution coated test strip and thin films on glass which could detect TNT in solution and vapour phase, respectively.

3. Thiocalix[4]arene-fluorescein based receptor for detecting CN^- and Cu^{2+} ions and construction of a sequential logic circuit

Among various anions, cyanide is well known for its toxic effects to both environment as well as biological systems.³⁸ The toxicity of cyanide is due to its tendency to bind with iron in cytochrome c oxidase which leads to hypoxia³⁹ and the extreme toxicity comes from gold mining, electroplating and tanning industries. On the other hand, copper is one of the essential transition metal ions present in the human body which plays an important role in

various physiological processes.⁴⁰ Copper is also vital trace element for the activities of enzymes. Unusual uptake of Cu^{2+} ions by mammals is known to cause Wilson's disease, gastrointestinal disease, hypoglycaemia, and infant liver damage.⁴¹ Therefore, monitoring the concentration of copper ions in environmental samples is of considerable importance for environment protection and human health. Keeping in view the significance of CN^- and Cu^{2+} ions, we have designed and synthesized a fluorescent probe based on thiacalix[4]arene with fluorescein moiety attached in it via imine linkage. Condensation of **29** with fluorescein monoaldehyde **30** in dry dichloromethane and absolute ethanol furnished the desired compound **31** in 47% yield (**Scheme 12**). The ^1H NMR spectrum of compound **31** shows three triplets (6 H, 4 H & 4 H) at 0.59, 3.60 and 3.77 ppm corresponding to the $-\text{CH}_3$, $-\text{NCH}_2$, and $-\text{OCH}_2$ protons, two multiplets (2 H each) at 1.04-1.06 and at 4.14-4.20 ppm which corresponds $-\text{OCH}_2$ and $-\text{CH}_2$ protons, two singlets (18 H each) at 1.18 and 1.31 ppm corresponding to the $-\text{C}(\text{CH}_3)_3$, one multiplet (4 H) at 6.51-6.61 ppm corresponding to

Scheme 12

aromatic protons, four singlets (4 H, 4 H, 1 H and 1 H) at 7.33, 7.57, 6.68 and 6.74 ppm corresponding to aromatic protons of thiacalix[4]arene and fluorescein moieties, three doublets (2 H each) at 6.97, 7.14 and 7.98 ppm corresponding to aromatic protons of fluorescein moiety, two triplets (2 H and 4 H) at 7.71 and 7.77 ppm corresponding to aromatic protons of fluorescein moiety, one singlet (2 H) at 9.05 ppm corresponding to the imino protons. The two phenolic protons labelled as H_a (red) and H_b (blue) appear at 10.19 of H_b proton is due to the fact that it is involved in intramolecular hydrogen bonding with closely situated imino nitrogen atom. The

molecular ion peak at $m/z = 1575.4897$ (M+1) in the MALDI-TOF spectrum corresponds to the condensation product **31**. These spectroscopic data corroborate the structure **31** for this compound.

The binding behaviour of compound **31** was studied toward different cations (Hg^{2+} , Pb^{2+} , Ba^{2+} , Cd^{2+} , Ag^+ , Zn^{2+} , Cu^{2+} , Ni^{2+} , Co^{2+} , Fe^{3+} , Fe^{2+} , K^+ , Mg^{2+} , Na^+ and Li^+) and anions (CN^- , F^- , Cl^- , Br^- , I^- , NO_3^- , AcO^- , H_2PO_4^- , SO_4^{2-}) by UV-vis and fluorescence spectroscopy. The UV-vis spectrum of compound **31** exhibited an absorption band at 258 nm. On addition of different metal ions, no new absorption band appears in the UV-vis spectrum which indicates that these metal ions do not interact with the compound **31** in the ground state. Among the various anion tested, a new absorption band is formed at 498 nm on addition of CN^- ions (**Figure 84**). The formation of the new absorption band at 498 nm is attributed to the opening of spirolactone ring of the fluorescein moiety. The fluorescence spectrum of receptor **26** does not exhibit any emission when excited at 490 nm. The addition of only cyanide ions (0-25 equiv) to the solution of receptor **31** results in the appearance of a new emission band at 540 nm (**Figure 85**) attributed to the spirolactone ring opening of fluorescein moiety. This nucleophilic attack leads to increased negative charge on nitrogen atom, which then abstracts proton from hydroxyl group of phenolic moiety leading to opening of spirolactone ring. The band at 540 nm increased and blue shifted to 528 nm with the increase in concentration of cyanide ions, which indicates that the nucleophilic addition is favourable at higher concentration of cyanide ions.

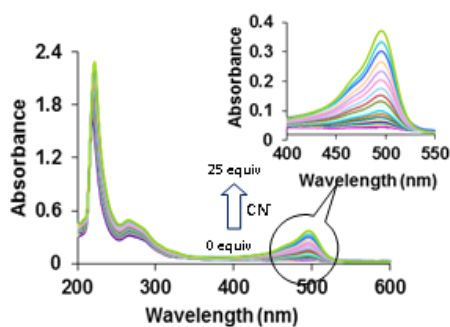


Figure 84: UV-vis spectra of **31** (5.0 μM) in the presence of CN^- anions (0-25 equiv) in $\text{CH}_3\text{CN}/\text{H}_2\text{O}$ (8:2, v/v) buffered with HEPES, pH = 7.0.

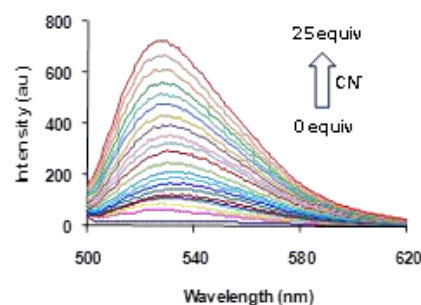


Figure 85: Fluorescence spectra of **31** (5.0 μM) in response to the presence of CN^- anions (0-25 equiv) in $\text{CH}_3\text{CN}/\text{H}_2\text{O}$ (8:2, v/v) buffered with HEPES, pH = 7.0; $\lambda_{\text{ex}} = 490$ nm.

To confirm the nucleophilic addition by cyanide, we carried out ^1H NMR studies of derivative **31** with TBACN in $\text{DMSO}-d_6$. The ^1H NMR spectrum of receptor **31** exhibits signals at 9.05, 10.19 and 14.49 ppm corresponding to the imino, H_a and H_b protons. On addition of cyanide ions to the receptor **31**, the signals corresponding to

the imino and hydroxyl protons at δ 9.05 and 14.49 ppm disappeared and the new signals corresponding to amino (-NH) and -CH(CN) protons appeared as singlet at 5.70 and 8.26 ppm. These changes in ^1H NMR spectra confirm the nucleophilic addition of cyanide and formation of cyanide adduct. The formation of cyanide adduct was further confirmed by ^{13}C NMR spectrum, with the appearance of a signal at 65.34, 98.57 and 181.36 ppm corresponding to carbon atom of amino (**Ca**), nitrile, and quinone moiety and disappearance of a signal at 166.78 ppm corresponding to imino carbon atom. In the MALDI- TOF mass spectrum a peak appeared at m/z 953.4421 which also confirmed the formation of adduct **31a**.

Further, we have checked binding behaviour of the adduct **31a** toward different cations. The decrease in absorption band at 498 nm (**Figure 86**) and complete quenching of fluorescence emission at 528 nm (**Figure 87**) clearly indicates that ring closing takes place

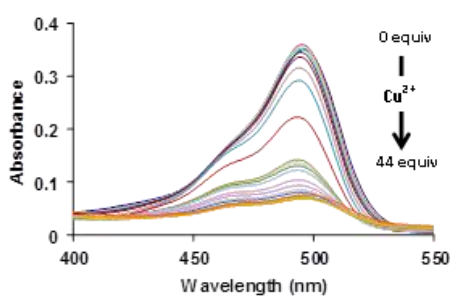


Figure 86: Absorbance spectra of **31a** in the presence of Cu^{2+} ions (0-44 equiv) in $\text{CH}_3\text{CN}/\text{H}_2\text{O}$ (8:2; v/v) buffered with HEPES, pH = 7.0.

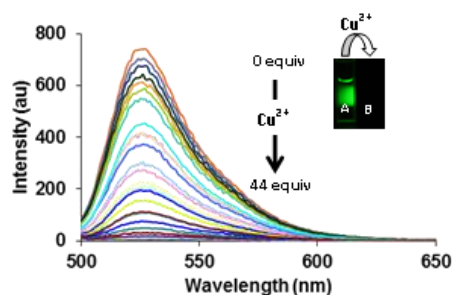


Figure 87: Fluorescence spectra of **31a** (5.0 μM) in response to the addition of Cu^{2+} ions (0-44 equiv) in $\text{CH}_3\text{CN}/\text{H}_2\text{O}$ (8:2; v/v); $\lambda_{\text{ex}} = 490$ nm. Inset showing the fluorescence change (A) before and (B) after the addition of Cu^{2+} ions.

in the presence of Cu^{2+} ions. No significant fluorescence quenching was observed with the addition of other metal ions. The formation of copper complex **26b** is also confirmed by mass spectrum in which a peak appears at $m/z = 877.7056$. Further addition of cyanide ions removes the copper from its binding site and facilitates the opening of spirolactone ring of the fluorescein moiety. Fitting the changes in the fluorescence spectra of adduct **31a** with Cu^{2+} ions (**Figure 87**), the nonlinear regression analysis program SPECFIT⁴² gave a good fit and demonstrated that a 1:2 stoichiometry (host: guest) was the most stable species in the solution with a binding constant of $(\log\beta) = 9.58$ with 0.05 error. Further, by considering the fluorescence intensity, a 43-fold emission enhancement at 528 nm was observed in the case of the adduct **31a**. The fluorescence quantum yield⁴³ of adduct **31a** system was calculated to

be 0.31 (at $\lambda_{em} = 528$ nm, $\lambda_{ex} = 490$ nm) which is greater than that of free receptor **31** (0.02). The detection limit⁴⁴ of receptor **31** for cyanide ions was found to be 1.911×10^{-7} mol L⁻¹ which is sufficiently low for the detection of cyanide ions found in many chemical systems.⁴⁵ Further, the addition of cyanide ions turned the original colourless solution of receptor **31** into greenish yellow immediately which could be easily seen by the naked eye. We have also checked the reversibility and reusability of chemosensor **31** with the alternate sequential addition of CN⁻ and Cu²⁺ ions which

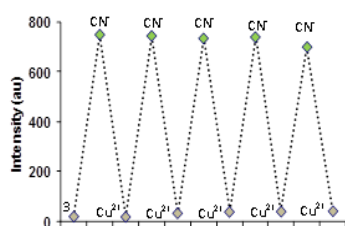


Figure 88: Reversible fluorescence signal changes of compound **31** (5 μ M) with sequential addition of CN⁻ and Cu²⁺.

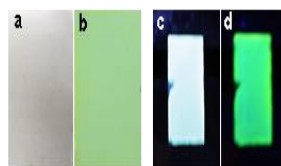


Figure 89: Colour and fluorescence changes of paper strips upon addition of cyanide; (a) Paper strips immersed into the solution of receptor **31**; (b) Colour change of molecule coated paper strips dipped into the solution of cyanide (10^{-3} M); (c) Paper strip 'a' under UV- illumination at 365 nm; (d) Paper strip 'b' under UV- illumination at 365 nm.

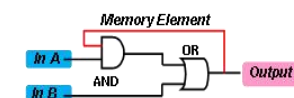


Table 1

Sr. No.	In A	In B	Output (528 nm)
1	0	0	0
2	1	0	0
3	0	1	1
4	1 (1 st)	1 (2 nd)	1
5	1 (2 nd)	1 (1 st)	0

Figure 90: Sequential logic circuit displaying memory unit with two inputs (In A and In B) and one output. Table 1 is the truth table for sequential logic circuit.

shows turn-on and turn-off cycles are reproducible while carrying out titration with CN⁻ and Cu²⁺ ions in an alternate manner (**Figure 88**). Further, for practical application, we prepared test strips coated with compound **31** were immersed into the solution of cyanide. A remarkable colour change from colourless to greenish yellow colouration was observed with naked eye. The green fluorescence was observed under the UV- illumination (**Figure 89**). Depending upon the different chemical inputs (CN⁻ and Cu²⁺) and fluorescent signals as outputs, a sequential logic circuit is constructed (**Figure 90**).

In summary, we synthesized a new thiacalix[4]arene-fluorescein based fluorescence turn-on probe for selective detection of CN⁻ ions. Further, the cyanide adduct was used for the detection copper ions. We also constructed a sequential logic circuit at molecular level and prepared paper strips for real life measurement.

List of publications

1. Terphenyl-phenanthroline conjugate as a Zn²⁺ sensor: H₂PO₄⁻ induced tuning of emission wavelength Vandana Bhalla, Ruchi Tejpal and Manoj Kumar **Dalton Trans.**, 2012,41, 10182

2. Triphenylene to supertriphenylene: New chemodosimeter for fluoride ions Vandana Bhalla, Hardev Singh, Harshveer Arora, Manoj Kumar **Sensors and Actuators B** **2012**, 171–172, 1007
3. Aggregates of a triphenylene based chemosensing ensemble for sensitive detection of cyanide ions in an aqueous medium Vandana Bhalla, Harshveer Arora and Manoj Kumar **Dalton Trans.**, **2013**, 42, 4450
4. Triphenylene derivatives: chemosensors for sensitive detection of nitroaromatic explosives Vandana Bhalla, Harshveer Arora, Hardev Singh and Manoj Kumar **Dalton Trans.**, **2013**, 42, 969
5. Fluorescent aggregates of AIEE active triphenylene derivatives for the sensitive detection of picric acid Harshveer Arora, Vandana Bhalla and Manoj Kumar **RSC Adv.**, **2015**, 5, 32637
6. A thiocalix[4]crown based chemosensor for Zn^{2+} and $H_2PO_4^-$: sequential logic operations at the molecular level Neetu Sharma, Shahi Imam Reja, Vandana Bhalla and Manoj Kumar **Dalton Trans.**, **2015**, 44, 6062

References

- ¹ L. Chen, J. Kim, T. Ishizuka, Y. Honsho, A. Saeki, S. Seki, H. Ihee, D. Jiang. *J. Am. Chem. Soc.* 2009, **131**, 7287.
- ² Grosby, G. A.; Demas, J. N. *J. Phys. Chem.*, 1971, **75**, 991.
- ³ D. Cai, R.D. Larsen and P. J. Reider, *Tetrahedron* 2002, 4285.
- ⁴ (a) E. G. McRae and M. J. Kasha, *Chem. Phys.* 1958, **28**, 721. (b) A. Mishra, R. K. Behera, P. K. Behera, B. K. Mishra and G. B. Behera, *Chem. Rev.* 2000, **100**, 1973
- ⁵ (a) Y. B. Ruan, A. F. Li, J. S. Zhao, J. S. Shen and Y. B. Jiang, *Chem. Commun.* 2010, **46**, 4938. (b) Y. Q. Weng, F. Yue, Y. R. Zhong and B. H. Ye, *Inorg. Chem.* 2007, **46**, 7749. (c) Y. Che, X. Yang, and L. Zang, *Chem. Commun.* 2008, 1413. (d) S. Gadde, E. K. Batchelor, J. P. Weiss, Y. Ling and A. E. Kaifer, *J. Am. Chem. Soc.* 2008, **130**, 17114.
- ⁶ H. Gampp, M. Maeder, C. J. Meyer and A. D. Zuberbuhler, *Talanta*, 1985, **32**, 95.
- ⁷ The blood serum was isolated by centrifugation of the fresh blood sample of a healthy volunteer after fasting at 4000 rpm for 20 min at 4 °C. The stock solution of blood serum was prepared by dissolving 100 µL of serum in 1 mL solution of HEPES buffer at pH = 7.0.
- ⁸ M. Tavasli, S. Bettington, M. R. Bryce, A. S. Batsanov and A. P. Monkman. *Synthesis*, 2005, **10**, 1619
- ⁹ R. Breslow, B. Jaus, R. Q. Kluttz and C. Z. Xia, *Tetrahedron*, 1982, **38**, 863.
- ¹⁰ J. Pommerehne, H. Vestweber, W. Guss, R. F. Mark, H. Bassler, M. Porsch and J. Daub, *Adv. Mater.*, 1995, **7**, 55
- ¹¹ (a) Principles of Fluorescence Spectroscopy, 2nd ed.; Lakowicz, J. R., Ed.; Kluwer Academic/Plenum Publishers: New York, 1999. (b) D. Zhao and T. M. Swager *Macromolecules*, 2005, **38**, 9377
- ¹² S. J. Toal and W. C. Trogler *J. Mater. Chem.*, 2006, **16**, 2871
- ¹³ Pernia, G. J.; Kilburn, J. D.; Essex, J. W.; Mortishire-Smith R. J.; Rowley, M. *J. Am. Chem. Soc.* 1996, **118**, 10220.
- ¹⁴ Du, X.; Wang, Z. Y. *Chem. Commun.* 2011, **47**, 4276.
- ¹⁵ Gierschner, J.; Park, S. Y. *J. Mater. Chem. C* 2013, **1**, 5818.
- ¹⁶ Wang, F.; Han, M. Y.; Mya, K. Y.; Wang Y.; Lai, Y. H. *J. Am. Chem. Soc.* 2005, **127**, 10350.
- ¹⁷ Tong, H.; Hong, Y.; Dong, Y.; Ren, Y.; Haussler, M.; Lam, J. W. Y.; Wong, K. S.; Tang, B. Z. *J. Phys. Chem. B* 2007, **111**, 2000.
- ¹⁸ Deams, J. N.; Grosby, G. A. *J. Phys. Chem.* 1971, **75**, 991.
- ¹⁹ Dong, S.; Li, Z.; J. Qin, *J. Phys. Chem. B* 2009, **113**, 434.

- ²⁰ (a) Wang, J.; Mei, J.; Yuan, W.; Lu, P.; Qin, A.; Sun, J.; Mac, Y.; Tang, B. Z. *J. Mater. Chem.* 2011, **21**, 4056. (b) Liu, J.; Zhong, Y.; Lu, P.; Hong, Y.; Lam, J. W. Y.; Faisal, M.; Yu, Y.; Wong, K. S.; Tang, B. Z. *Polym. Chem.* 2010, **1**, 426. (c) Zhao, D.; Swager, T. M. *Macromolecules* 2005, **38**, 9377.
- ²¹ (a) Liu, X.; Zhang, X.; Lu, R.; Xue, P.; Xu, D.; Zhou, H. *J. Mater. Chem.* 2011, **21**, 8756. (b) Ding, Z.; Zhao, Q.; Xing, R.; Wang, X. G.; Ding, J.; Wang, L.; Han, Y. *J. Mater. Chem. C* 2013, **1**, 786.
- ²² Prez, G.V.; Prez, A.L. *J. Chem. Educ.* 2000, **77**, 910.
- ²³ (a) Roy, B.; Bar, A. K.; Gole, B.; Mukherjee, P. S. *J. Org. Chem.* 2013, **78**, 1306. (b) Vishnoi, P.; Walawalkar, M. G.; Sen, S.; Datta, A.; Patwari, G. N.; Murugavel, R. *Phys. Chem. Chem. Phys.* 2014, **16**, 10651.
- ²⁴ (a) Vajpayee, V.; Kim, H.; Mishra, A.; Mukherjee, P. S.; Stang, P. J.; Lee, M. H.; Kim, H. K.; Chi, K.-W. *Dalton Trans.*, 2011, **40**, 3112. (b) Venkatramaiah, N.; Kumar, S.; Patil, S. *Chem. Commun.*, 2012, **48**, 5007.
- ²⁵ Serizawa, T.; Hirai, Y.; Aizawa, M. *Langmuir*, 2009, **25**, 12229.
- ²⁶ Sun, X.; Jiang, X.; Dong, S.; Wang, E. *Macromol. Rapid Commun.* 2003, **24**, 1024.
- ²⁷ Puvvada, S.; Baral, S.; Chow, G. M.; Qadri, S. B.; Ratna, B. R. *J. Am. Chem. Soc.* 1994, **116**, 2135.
- ²⁸ Nadagouda, M. N.; Varma, R. S. *Green Chem.*, 2008, **10**, 859.
- ²⁹ Aslam, M.; Fu, L.; Su, M.; Vijayamohanamb, K.; Dravid, V. P. *J. Mater. Chem.* 2004, **14**, 1795.
- ³⁰ (a) Zhang, X.; Su, Z. H. *Adv. Mater.* 2012, **24**, 4574. (b) Tang, S. C.; Vongehr, S.; Meng, X. K. *J. Mater. Chem.* 2010, **20**, 5436. (c) Sun, Y. G.; Lei, C. H. *Chem. Int. Ed.* 2009, **48**, 6824. (d) Li, H. Q.; Han, L. N.; Cooper-White, J.; Kim, I. *Green Chem.* 2012, **14**, 586. (e) Li, J.; Liu, C. Y.; Liu, Y. *J. Mater. Chem.* 2012, **22**, 8426.
- ³¹ (a) Maruyama, S.; Sato, K.; Iwahashi, H. *Chem. Lett.* 2010, **39**, 714. (b) Achalkumar, A. S.; Hiremath, U. S.; Rao, D. S. S.; Prasad, S. K.; Yelamaggad, C. V. *J. Org. Chem.* 2003, **78**, 527. (c) Judele, R.; Laschat, S.; Baro, A.; Nimtz, M. *Tetrahedron* 2006, **62**, 9681.
- ³² Jang, S.; Kim, S.G.; Jung, D.; Kwon, H.; Song, J.; Cho, S.; Ko, Y. C.; Sohn, H. *Bull. Korean Chem. Soc.* 2006, **27**, 12.
- ³³ (a) Hamuro, Y.; Geib, S. J.; Hamilton, A. D. *J. Am. Chem. Soc.* 1997, **119**, 10587. (b) Xiao, S.; Myers, M.; Miao, Q.; Sanaur, S.; Pang, K.; Steigerwald M. L.; Nuckolls, C. *Angew. Chem., Int. Ed.* 2005, **44**, 7390. (c) Liu, W. J.; Zhou, Y.; Ma, Y.; Cao, Y.; Wang, J.; Pei, J. *Org. Lett.* 2007, **9**, 4187.
- ³⁴ Deams, J. N.; Grosby, G. A. *J. Phys. Chem.* 1971, **75**, 991.
- ³⁵ Liu, J.; Zhong, Y.; Lu, P.; Hong, Y.; Lam, J. W. Y.; Faisal, M.; Yu, Y.; Wong, K. S.; Tang, B. Z. *Polym. Chem.* 2010, **1**, 426.
- ³⁶ (a) Ding, Z.; Zhao, Q.; Xing, R.; Wang, X. G.; Ding, J.; Wang, L.; Han, Y. *J. Mater. Chem. C* 2013, **1**, 786. (b) Liu, X.; Zhang, X.; Lu, R.; Xue, P.; Xu, D.; Zhou, H. *J. Mater. Chem.* 2011, **21**, 8756.
- ³⁷ Zhao, D.; Swager T. M. *Macromolecules* 2005, **38**, 9377.
- ³⁸ (a) Z. Guo, S. W. Nam, S. Park and J. Yoon, *Chem. Sci.*, 2012, **3**, 2760; (b) Z. Xu, Chen, H. N. Kim and J. Yoon, *Chem. Soc. Rev.*, 2010, **39**, 127; (c) X. Chen, S. W. Nam, G. H. Kim, N. Song, Y. Jeong, I. Shin, S. K. Kim, J. Kim, S. Park and J. Yoon, *Chem. Commun.*, 2010, **46**, 8953.
- ³⁹ (a) K. Kulig, Cyanide Toxicity, U.S. Department of Health and Human Services, Atlanta, GA, 1991; (b) S. Baskin and T. Brewer, in *Medical Aspects of Chemical and Biological Warfare*, ed. F. Sidell, E. T. Takafuji and D. R. Franz, TMMPublication, Washington, DC, 1997, pp. 271–286.
- ⁴⁰ (a) D. Y. Sasaki, D. R. Shnek, D. W. Pack and F. H. Arnold, *Angew. Chem., Int. Ed. Engl.*, 1995, **34**, 905; (b) R. Krämer, *Angew. Chem., Int. Ed.*, 1998, **37**, 772; (c) P. Grandini, F. Mancin, P. Tecilla, P. Scrimin and U. Tonellato, *Angew. Chem., Int. Ed.*, 1999, **38**, 3061.
- ⁴¹ (a) N. Kumar, *Mayo Clin. Proc.*, 2006, **81**, 1371; (b) B. Sarkar, *In Metal Ions in Biological Systems*; H. Siegel and A. Siegel, Eds.; Marcel Dekker: New York, 1981; **Vol. 12**, p 233.
- ⁴² H. Gampp, M. Maeder, C. J. Meyer and A. D. Zhuberbulher, *Talanta*, 1985, **32**, 95.
- ⁴³ J. N. Demas and G. A. Crosby, *J. Phys. Chem.*, 1971, **75**, 991.
- ⁴⁴ S. Goswami, S. Das, K. Aich, D. Sarkar, T. K. Mondal, C. K. Quah, H.-K. Fun, *Dalton Trans.*, 2013, **42**, 15113.

⁴⁵ G. C. Miller and A. Pritsos, Cyanide: social, industrial and economic aspects, Proceeding of the TMS Annual Meeting, 2001, p. 73.